

Ordered states of undoped AB bilayer graphene: bias induced cascade of transitions

A.V. Rozhkov,¹ A.O. Sboychakov,¹ and A.L. Rakhmanov¹

¹*Institute for Theoretical and Applied Electrodynamics,
Russian Academy of Sciences, 125412 Moscow, Russia*

(Dated: February 13, 2026)

Using mean-field theory, we determine the electronic phase diagram of undoped AB-stacked bilayer graphene in the presence of a transverse electric field. In addition to multiple competing electronic instabilities characterized by excitonic order parameters, our framework incorporates the long-range Coulomb energy associated with interlayer polarization. This long-range interaction plays a crucial role, as it significantly influences both the structure and the relative energies of the competing ordered states. We derive a set of self-consistency equations and solve them both numerically and analytically. Our findings reveal that, as the bias field is varied, the bilayer undergoes a cascade of first-order transitions between several ordered insulating phases for which order-parameter structures are explicitly identified. Some of these phases are characterized by two inequivalent single-particle gaps, whose magnitudes depend on the valley and spin quantum numbers. Field-driven transitions are accompanied by discontinuous and non-monotonic variations of the single-electron gap. We relate our results to Hartree-Fock numerical calculations and to experimental research, including observations of fractional metallic phases that emerge upon doping the bilayer system.

I. INTRODUCTION

Ordered phases of electronic liquid in bilayer and multilayer graphene structures are studied^{1,2} for more than a decade, both experimentally^{3–15} and theoretically^{16–30}. Recent renewed interest in this subject is motivated by experimental observations of fractional metallic phases in doped multilayer samples^{12,14}, for which fractional metallicity had been theoretically predicted earlier, including half-metal^{26,27} and quarter-metal states³⁰.

It is reasonable to expect that the fractional metallicity of doped phases may be linked to the properties of their undoped parent states. Accordingly, gaining insight into the physics of the undoped phases may be regarded as an important priority in this context. Motivated by these considerations, we formulate a simple, analytically tractable mean field scheme that describes competition of various ordered state in an undoped sample of AB-stacked bilayer graphene (AB-BLG) placed in transverse electric field.

Our work builds on a substantial body of prior theoretical research, such as Refs. 16, 17, 22, and 26. Extending these studies, we aim for a framework that balances methodological clarity with comprehensive integration of the key elements governing electronic order in AB-BLG. Beside fairly common two-band Hamiltonian in the presence of transverse electric field, augmented by exchange electron-electron interaction, we incorporate charging (Hartree) energy associated with inter-layer polarization. Also, four distinct order parameters (one per valley, per spin projection) are explicitly accounted for in our calculations. This order parameters quadruplet enables us to distinguish and keep track of several, rather dissimilar, ordered states of undoped AB-BLG.

The model is studied within the variational formulation of the mean-field approximation. The derived self-

consistency equations are solved analytically and numerically, allowing the phase diagram to be constructed. It reveals a bias-driven cascade of first-order transitions among ordered insulating phases, accompanied by a non-monotonic behavior of the single-particle gap. Another notable result of this study is the identification of several universal features of the phase diagram.

The four order parameters respond differently to the bias: at finite field, their absolute values may be non-identical, signifying that the gaps in different fermion sectors are non-identical. This spectral feature has important consequences for the formation of the fractional-metal states at finite doping.

Our analytical results are in good agreement with numerical studies, such as Refs. 22 and 26. In particular, we show that data obtained from computationally intensive Hartree-Fock calculations can be effectively reproduced using relatively straightforward analytical methods. Encouragingly, previously unknown universal features, which we identified in our study, are clearly visible in the Hartree-Fock phase diagram.

We compare our results with experiment of Ref. 31. It appears that the data partially consistent with the calculations presented below. The relation between the model and experiment is discussed.

The paper is organized as follows. In Sec. II we explain our model's structure. In Sec. III the mean field theory is formulated, and the self-consistency equations are derived. Thermodynamic phases compatible with the self-consistency equations are discussed in Sec. IV. The phase diagram is mapped in Sec. V. Discussion of the results is in Sec. VI. Conclusions are in Sec. VII. Several calculations are relegated to Appendices.

II. MODEL

A. Tight-binding model

The unit cell of the Bernal-type or AB bilayer graphene (AB-BLG) includes four carbon atoms on two sublattices. The carbon atoms in the sublattice B of the top layer are located right above the atoms of the sublattice A of the lower layer (such atoms are called dimers), while the atoms in the sublattice A of the top layer are located above centers of the hexagons formed by the atoms of the lower layer (non-dimer sites). The elementary translation vectors for the AB-BLG can be chosen as $\mathbf{a}_{1,2} = a(\sqrt{3}, \mp 1)/2$, where $a = 2.46\text{\AA}$ is the elementary unit length. The inter-layer distance for AB-BLG is $d = 3.35\text{\AA}$.

Below we consider an undoped gated sample of AB-BLG. The model Hamiltonian can be presented as a sum of two terms

$$H = H_0 + H_{\text{int}}, \quad (1)$$

where the first term is the single-particle Hamiltonian, while the second term represents the Coulomb electron-electron interaction. We start with a short discussion of the single-electron term

$$H_0 = \sum_{\mathbf{k}\sigma} \psi_{\mathbf{k}\sigma}^\dagger \mathcal{H}_{\mathbf{k}} \psi_{\mathbf{k}\sigma}, \quad (2)$$

where the four-component operator-valued spinor $\psi_{\mathbf{k}\sigma}^\dagger$ is defined as

$$\psi_{\mathbf{k}\sigma}^\dagger = (d_{\mathbf{k}1A\sigma}^\dagger, d_{\mathbf{k}1B\sigma}^\dagger, d_{\mathbf{k}2A\sigma}^\dagger, d_{\mathbf{k}2B\sigma}^\dagger), \quad (3)$$

$d_{\mathbf{k}ia\sigma}^\dagger$ and $d_{\mathbf{k}ia\sigma}$ are the creation and annihilation operators of the electrons with momentum \mathbf{k} in the layer $i(=1, 2)$, in the sublattice $a(=A, B)$ with spin projection $\sigma(=\uparrow, \downarrow)$, and the 4×4 matrix $\mathcal{H}_{\mathbf{k}}$ equals

$$\mathcal{H}_{\mathbf{k}} = \begin{pmatrix} e\Phi/2 & -tf_{\mathbf{k}} & 0 & t_0 \\ -tf_{\mathbf{k}}^* & e\Phi/2 & 0 & 0 \\ 0 & 0 & -e\Phi/2 & -tf_{\mathbf{k}} \\ t_0 & 0 & -tf_{\mathbf{k}}^* & -e\Phi/2 \end{pmatrix}. \quad (4)$$

Here e is the electron charge, Φ is the bias voltage, and the function $f_{\mathbf{k}}$ is

$$f_{\mathbf{k}} = e^{i\mathbf{k}\delta} [1 + e^{-i\mathbf{k}\mathbf{a}_1} + e^{-i\mathbf{k}\mathbf{a}_2}], \quad (5)$$

where $\delta = (\mathbf{a}_1 + \mathbf{a}_2)/3$, parameter $t = 2.7\text{ eV}$ is the in-plane nearest-neighbor hopping amplitude, and $t_0 = 0.4\text{ eV}$ is the out-of-plane hopping amplitude between nearest-neighbor dimer sites¹.

The spectrum of the single-particle Hamiltonian (4) consists of four bands

$$\varepsilon_{\mathbf{k}}^{(S)} = \mp \sqrt{t_{\mathbf{k}}^2 + \frac{e^2\Phi^2}{4} + \frac{t_0^2}{2} \mp \sqrt{t_{\mathbf{k}}^2(e^2\Phi^2 + t_0^2) + \frac{t_0^4}{4}}}, \quad (6)$$

two hole bands $\varepsilon_{\mathbf{k}}^{(1,2)}$, and two electron bands $\varepsilon_{\mathbf{k}}^{(3,4)}$. Here $S = 1, \dots, 4$ and $t_{\mathbf{k}} = t|f_{\mathbf{k}}|$. When $e\Phi = 0$, the bands $\varepsilon_{\mathbf{k}}^{(2)}$ and $\varepsilon_{\mathbf{k}}^{(3)}$ touch each other at the Dirac points $\mathbf{K}_1 = (0, 4\pi/3a)$ and $\mathbf{K}_{-1} = -\mathbf{K}_1$. At non-zero $e\Phi$ a single-particle gap opens, and the undoped AB-BLG becomes an insulator.

The bispinor wave functions

$$\Psi_{\mathbf{k}}^{(S)} = (\Psi_{\mathbf{k}1A}^{(S)}, \Psi_{\mathbf{k}1B}^{(S)}, \Psi_{\mathbf{k}2A}^{(S)}, \Psi_{\mathbf{k}2B}^{(S)}) \quad (7)$$

correspond to the eigenvalues $\varepsilon_{\mathbf{k}}^{(S)}$. The analytical formulas for $\Psi_{\mathbf{k}}^{(S)}$ are quite cumbersome, and it is often more practical to evaluate them numerically.

At a fixed $e\Phi$, it is convenient to introduce a new operator basis according to

$$d_{\mathbf{k}ia\sigma} = \sum_S \Psi_{\mathbf{k}ia\sigma}^{(S)} \tilde{\gamma}_{\mathbf{k}S\sigma}, \quad (8)$$

where operator $\tilde{\gamma}_{\mathbf{k}S\sigma}$ (operator $\tilde{\gamma}_{\mathbf{k}S\sigma}^\dagger$) destroys (creates) an electron in the eigenstate S with momentum \mathbf{k} and spin σ . The single-particle Hamiltonian

$$H_0 = \sum_{\mathbf{k}S\sigma} \varepsilon_{\mathbf{k}}^{(S)} \tilde{\gamma}_{\mathbf{k}S\sigma}^\dagger \tilde{\gamma}_{\mathbf{k}S\sigma} \quad (9)$$

is diagonal in this operator basis.

Here we are interested in the low-temperature orderings of the AB-BLG. The characteristic energy scale for such phenomena does not exceed several meV, which is much smaller not only t , but t_0 as well. We additionally assume that

$$|e\Phi| \lesssim t_0, \quad (10)$$

which is always fulfilled in experiment. In this regime, the two-band approximation is appropriate: the bands $\varepsilon_{\mathbf{k}}^{(1,4)}$ are ignored, and only bands $\varepsilon_{\mathbf{k}}^{(2,3)}$, which are the closest to the Fermi level, are kept in the formalism.

As a further simplification, only single-electron states sufficiently close to the Dirac points are retained. For proper enumeration of such states, it is convenient to introduce reciprocal space cutoff $q_0 = 2t_0/\sqrt{3}ta < |\mathbf{K}_1 - \mathbf{K}_{-1}|/2$, and valley index $\xi = \pm 1$. If \mathbf{k} satisfies the inequality $|\mathbf{k} - \mathbf{K}_\xi| < q_0$, a single-electron state with such a momentum is assigned to valley ξ . In a specific valley, we count the electron momentum from the corresponding Dirac point $\mathbf{k} \rightarrow \mathbf{k} - \mathbf{K}_\xi$.

In the two-band framework, the operator basis introduced by Eq. (8) is not always convenient: operators $\tilde{\gamma}_{\mathbf{k}S\sigma}$ depend on transverse potential $e\Phi$, which may lead to awkward intermediate formulas, and they do not have explicit valley designations. We address these matters by defining new operators in the following manner. Observe that in the case of $e\Phi = 0$, in the low-energy approximation we have simple analytical formulas for the

eigenvectors $\Psi_{\mathbf{k}ia\sigma}^{(S)}$ [see also Eq. (21) in Ref. 32]

$$\begin{aligned}\Psi_{\mathbf{k}ia\sigma}^{(2)} &= \frac{1}{\sqrt{2}} (0, \psi_{\mathbf{k}}^*, \psi_{\mathbf{k}}, 0)^T, \\ \Psi_{\mathbf{k}ia\sigma}^{(3)} &= \frac{1}{\sqrt{2}} (0, -\psi_{\mathbf{k}}^*, \psi_{\mathbf{k}}, 0)^T,\end{aligned}\quad (11)$$

where $\psi_{\mathbf{k}} = \exp(i\pi/2 - i\xi\phi_{\mathbf{k}})$ and $\phi_{\mathbf{k}}$ is the polar angle for vector \mathbf{k} . Then, using Eq. (8) we obtain for non-dimer sites

$$d_{\mathbf{k}1B\xi\sigma} = \frac{-ie^{i\xi\phi_{\mathbf{k}}}}{\sqrt{2}} (\gamma_{\mathbf{k}2\xi\sigma} - \gamma_{\mathbf{k}3\xi\sigma}), \quad (12)$$

$$d_{\mathbf{k}2A\xi\sigma} = \frac{ie^{-i\xi\phi_{\mathbf{k}}}}{\sqrt{2}} (\gamma_{\mathbf{k}2\xi\sigma} + \gamma_{\mathbf{k}3\xi\sigma}), \quad (13)$$

where $\gamma_{\mathbf{k}S\xi\sigma}$ are the operators $\tilde{\gamma}_{\mathbf{k}S\sigma}$ at $e\Phi = 0$, localized at specific valley ξ . Thus, at $e\Phi = 0$, the Hamiltonian can be approximated as ($\hbar = 1$)

$$H_0 = \sum_{\mathbf{k}\xi\sigma} \varepsilon_{\mathbf{k}} \left(\gamma_{\mathbf{k}3\xi\sigma}^\dagger \gamma_{\mathbf{k}3\xi\sigma} - \gamma_{\mathbf{k}2\xi\sigma}^\dagger \gamma_{\mathbf{k}2\xi\sigma} \right), \quad (14)$$

where $\varepsilon_{\mathbf{k}} = v_F^2 \mathbf{k}^2 / t_0$ and $v_F = \sqrt{3}at/2$.

To account for a non-zero $e\Phi$, we should add the term $e\Phi(\rho_{10} - \rho_{20})/2$ in the Hamiltonian, where ρ_{i0} is the density operator in the layer $i = 1, 2$ according to

$$\rho_{i\mathbf{k}} = \sum_{\mathbf{q}\xi\sigma} \left(d_{\mathbf{q}+\mathbf{k}iA\xi\sigma}^\dagger d_{\mathbf{q}iA\xi\sigma} + d_{\mathbf{q}+\mathbf{k}iB\xi\sigma}^\dagger d_{\mathbf{q}iB\xi\sigma} \right), \quad (15)$$

evaluated at small wave vector $\mathbf{k} \rightarrow 0$ or in terms of the band operators

$$\rho_{10} - \rho_{20} = - \sum_{\mathbf{k}\xi\sigma} \left(\gamma_{\mathbf{k}2\xi\sigma}^\dagger \gamma_{\mathbf{k}3\xi\sigma} + \gamma_{\mathbf{k}3\xi\sigma}^\dagger \gamma_{\mathbf{k}2\xi\sigma} \right). \quad (16)$$

Therefore, the Hamiltonian H_0 becomes

$$H_0 = \sum_{\mathbf{k}\xi\sigma} \left(\gamma_{\mathbf{k}2\xi\sigma}^\dagger, \gamma_{\mathbf{k}3\xi\sigma}^\dagger \right) \begin{pmatrix} -\varepsilon_{\mathbf{k}} & -\frac{e\Phi}{2} \\ -\frac{e\Phi}{2} & \varepsilon_{\mathbf{k}} \end{pmatrix} \begin{pmatrix} \gamma_{\mathbf{k}2\xi\sigma} \\ \gamma_{\mathbf{k}3\xi\sigma} \end{pmatrix}. \quad (17)$$

The spectrum of the Hamiltonian (17) is

$$\varepsilon_{\mathbf{k}}^{(2,3)} = \mp \sqrt{\varepsilon_{\mathbf{k}}^2 + \frac{e^2\Phi^2}{4}}. \quad (18)$$

This Hamiltonian is invariant under action of the group

$$G = \mathrm{U}(2) \times \mathrm{U}(2) \quad (19)$$

that transforms the band operators according to

$$\gamma_{\mathbf{k}s\xi\sigma} = \sum_{\sigma'} u_{\sigma\sigma'}^\xi \gamma_{\mathbf{k}s\xi\sigma'}, \quad (20)$$

where $u_{\sigma\sigma'}^\xi$ are matrix elements of a 2×2 unitary matrix \hat{U}_ξ . This transformation is more general than the usual spin-rotation symmetry: it allows for an independent spin rotation in each valley.

B. Interaction Hamiltonian

We model the interaction Hamiltonian as follows

$$\begin{aligned}H_{\mathrm{int}} &= \frac{1}{2N_c} \sum_{\mathbf{k}} (V_{\mathbf{k}}^{11} \rho_{1\mathbf{k}} \rho_{1-\mathbf{k}} + V_{\mathbf{k}}^{22} \rho_{2\mathbf{k}} \rho_{2-\mathbf{k}} \\ &\quad + V_{\mathbf{k}}^{12} \rho_{1\mathbf{k}} \rho_{2-\mathbf{k}} + V_{\mathbf{k}}^{21} \rho_{2\mathbf{k}} \rho_{1-\mathbf{k}}),\end{aligned}\quad (21)$$

where N_c is the number of unit cells in a sample, and $V_{\mathbf{k}}^{ij}$ is the screened Coulomb potential that accounts for interaction between electrons in i -th and j -th layers. Note also that we neglect the electron scattering with large momentum transfer and below is assumed that

$$|\mathbf{k}| \ll |\mathbf{K}_1|. \quad (22)$$

At small \mathbf{k} , one can write for the “bare” Coulomb interaction:

$$V_{\mathbf{k}}^{11} = V_{\mathbf{k}}^{22} = \frac{2\pi e^2}{\epsilon S_0 |\mathbf{k}|}, \quad (23)$$

$$V_{\mathbf{k}}^{12} = V_{\mathbf{k}}^{21} = \frac{2\pi e^2}{\epsilon S_0 |\mathbf{k}|} e^{-|\mathbf{k}|d} \approx V_{\mathbf{k}}^{11} - \frac{2\pi e^2 d}{\epsilon S_0}, \quad (24)$$

where ϵ is a substrate permittivity and $S_0 = \sqrt{3}a^2/2$ is the area of the graphene unit cell.

Now we re-write the Hamiltonian (21) in the form

$$H_{\mathrm{int}} = H_{\mathrm{int}}^{\mathrm{cap}} + \tilde{H}_{\mathrm{int}}, \quad (25)$$

splitting the interaction in “Hartree” term, $H_{\mathrm{int}}^{\mathrm{cap}}$ at $\mathbf{k} = 0$ and “Hartree-Fock” term

$$\begin{aligned}\tilde{H}_{\mathrm{int}} &= \frac{1}{2N_c} \sum'_{\mathbf{k}} (V_{\mathbf{k}}^{11} \rho_{1\mathbf{k}} \rho_{1-\mathbf{k}} + V_{\mathbf{k}}^{22} \rho_{2\mathbf{k}} \rho_{2-\mathbf{k}} \\ &\quad + V_{\mathbf{k}}^{12} \rho_{1\mathbf{k}} \rho_{2-\mathbf{k}} + V_{\mathbf{k}}^{21} \rho_{2\mathbf{k}} \rho_{1-\mathbf{k}}),\end{aligned}\quad (26)$$

where the prime at the summation sign implies that $\mathbf{k} \neq 0$. The contribution at $\mathbf{k} = 0$ is simply a capacitive electrostatic energy

$$H_{\mathrm{int}}^{\mathrm{cap}} = -\frac{\mathcal{E}_0}{2N_c} \rho_{10} \rho_{20}, \quad (27)$$

where

$$\mathcal{E}_0 = \frac{4\pi e^2 d}{S_0 \epsilon} \approx \frac{116}{\epsilon} \text{ eV} \approx \frac{43t}{\epsilon}. \quad (28)$$

Beside the capacitance term, there is, of course, another Hartree contribution associated with the long-range Coulomb force [see Eqs. (23)]. It is proportional to $V_{\mathbf{k}}^{11}$ in the limit $\mathbf{k} \rightarrow 0$. Clearly, this is a divergent quantity whose role is to enforce total electroneutrality of the sample. Thus, we can write

$$(\rho_{10} + \rho_{20}) = 4N_c. \quad (29)$$

In other words, we always work within the subspace where the operator $(\rho_{10} + \rho_{20})$ has eigenvalue $4N_c$. This allows us to re-write $H_{\text{int}}^{\text{cap}}$ as follows

$$H_{\text{int}}^{\text{cap}} = -2\mathcal{E}_0 N_c + \frac{\mathcal{E}_0}{8N_c}(\rho_{10} - \rho_{20})^2. \quad (30)$$

It is necessary to express \tilde{H}_{int} and $H_{\text{int}}^{\text{cap}}$ in terms of the band operators. The term \tilde{H}_{int} is transformed first. We start by calculating $V_{\mathbf{k}}^{ij}$ at $\mathbf{k} \neq 0$ using the random phase approximation. This allows us to account for many-body screening effects³². The potentials $V_{\mathbf{k}}^{ij}$ decrease at large transferred momentum. This justifies us restricting ourselves to small transferred momentum limit (22).

According to definitions (8) and (15) we introduce projected coupling constants as

$$\begin{aligned} \Gamma_{\mathbf{k}\mathbf{k}'}^{(1)} &= \sum_{ij} \left(\sum_{a\sigma} \Psi_{\mathbf{k}ia\sigma}^{(2)*} \Psi_{\mathbf{k}'ia\sigma}^{(2)} \right) V_{\mathbf{k}-\mathbf{k}'}^{ij} \left(\sum_{b\sigma'} \Psi_{\mathbf{k}jb\sigma'}^{(3)} \Psi_{\mathbf{k}'jb\sigma'}^{(3)*} \right), \\ \Gamma_{\mathbf{k}\mathbf{k}'}^{(2)} &= \sum_{ij} \left(\sum_{a\sigma} \Psi_{\mathbf{k}ia\sigma}^{(2)*} \Psi_{\mathbf{k}'ia\sigma}^{(3)} \right) V_{\mathbf{k}-\mathbf{k}'}^{ij} \left(\sum_{b\sigma'} \Psi_{\mathbf{k}jb\sigma'}^{(3)} \Psi_{\mathbf{k}'jb\sigma'}^{(2)*} \right), \end{aligned} \quad (31)$$

and write down the Hamiltonian \tilde{H}_{int} in terms of the band operators $\tilde{\gamma}_{\mathbf{k}S\sigma}$, $\tilde{\gamma}_{\mathbf{k}S\sigma}^\dagger$

$$\begin{aligned} \tilde{H}_{\text{int}} = -\frac{1}{2N_c} \sum_{\mathbf{k}\mathbf{k}'\sigma\sigma'} & \left(\tilde{\gamma}_{\mathbf{k}2\sigma}^\dagger \tilde{\gamma}_{\mathbf{k}3\sigma'} \Gamma_{\mathbf{k}\mathbf{k}'}^{(1)} \tilde{\gamma}_{\mathbf{k}'3\sigma'}^\dagger \tilde{\gamma}_{\mathbf{k}'2\sigma} + \right. \\ & \left. \tilde{\gamma}_{\mathbf{k}2\sigma}^\dagger \tilde{\gamma}_{\mathbf{k}3\sigma'} \Gamma_{\mathbf{k}\mathbf{k}'}^{(2)} \tilde{\gamma}_{\mathbf{k}'2\sigma'}^\dagger \tilde{\gamma}_{\mathbf{k}'3\sigma} \right) + \text{H.c.} \end{aligned} \quad (32)$$

Here we only kept the terms responsible for the gap opening (at $\Phi = 0$). The coupling constants satisfy the relations

$$\Gamma_{\mathbf{k}\mathbf{k}'}^{(1)} = \Gamma_{\mathbf{k}'\mathbf{k}'}^{(1)*}, \quad \Gamma_{\mathbf{k}\mathbf{k}'}^{(2)} = \Gamma_{\mathbf{k}'\mathbf{k}'}^{(2)}. \quad (33)$$

Among these two, $\Gamma_{\mathbf{k}\mathbf{k}'}^{(1)}$ is responsible for the direct coupling, while $\Gamma_{\mathbf{k}\mathbf{k}'}^{(2)}$ represents the umklapp scattering.

Note that the definition (26) of \tilde{H}_{int} excludes zero-momentum terms. In the context of Eq. (32) this constraint is equivalent to the condition $\mathbf{k} \neq \mathbf{k}'$. However, there is no singularity at $\mathbf{k} = \mathbf{k}'$ in the case of the screened interaction. Thus, we can ignore this restriction, and assume everywhere that summations over \mathbf{k} and \mathbf{k}' in Eq. (32) (and related expressions) are independent of each other.

The condition (22) allows us to introduce valleys in our description of the interaction Hamiltonian, as it was done for H_0 . As a result, we have

$$\tilde{H}_{\text{int}} \approx \sum_{\xi} \tilde{H}_{\text{int}}^{\xi}, \quad (34)$$

$$\begin{aligned} \tilde{H}_{\text{int}}^{\xi} = -\frac{1}{2N_c} \sum_{\mathbf{k}\mathbf{k}'\sigma\sigma'} & \left(\gamma_{\mathbf{k}2\xi\sigma}^\dagger \gamma_{\mathbf{k}3\xi\sigma'} \Gamma_{\mathbf{k}\mathbf{k}'}^{(1)} \gamma_{\mathbf{k}'3\xi\sigma'}^\dagger \gamma_{\mathbf{k}'2\xi\sigma} + \right. \\ & \left. \gamma_{\mathbf{k}2\xi\sigma}^\dagger \gamma_{\mathbf{k}3\xi\sigma'} \Gamma_{\mathbf{k}\mathbf{k}'}^{(2)} \gamma_{\mathbf{k}'2\xi\sigma'}^\dagger \gamma_{\mathbf{k}'3\xi\sigma} \right) + \text{H.c.} \end{aligned} \quad (35)$$

Here \mathbf{k} and \mathbf{k}' are limited to a vicinity of \mathbf{K}_ξ . Note that Hamiltonian (35) is written in terms of operators $\gamma_{\mathbf{k}S\xi\sigma}$ instead of operators $\tilde{\gamma}_{\mathbf{k}S\sigma}$ [as in Eq. (32)]. In this case, the wave functions $\Psi_{\mathbf{k}ia\sigma}^{(S)}$ in Eq. (31) are given by Eq. (11). Our \tilde{H}_{int} has same-valley terms only. Such a simplification excludes some more exotic order parameters (the so-called Kekulé-like orders), which we believe is justified. Indeed, while various Kekulé-like phases are considered in theoretical literature^{18,21,23,33-35} as a mathematical possibility, detailed calculations often demonstrate that they do not become ground state under realistic conditions^{23,33}.

It is convenient to define an operator-valued 2×2 matrix $\hat{\Xi}_{\mathbf{k}\xi}$ whose matrix elements are

$$\Xi_{\mathbf{k}\xi}^{\sigma\sigma'} = \gamma_{\mathbf{k}3\xi\sigma}^\dagger \gamma_{\mathbf{k}2\xi\sigma'}, \quad [\Xi_{\mathbf{k}\xi}^{\dagger}]^{\sigma\sigma'} = \gamma_{\mathbf{k}2\xi\sigma}^\dagger \gamma_{\mathbf{k}3\xi\sigma'}. \quad (36)$$

Then Eq. (35) can be re-written as

$$\tilde{H}_{\text{int}}^{\xi} = -\frac{1}{2N_c} \sum_{\mathbf{k}\mathbf{k}'} \text{Tr} \left(\hat{\Xi}_{\mathbf{k}\xi}^\dagger \Gamma_{\mathbf{k}\mathbf{k}'}^{(1)} \hat{\Xi}_{\mathbf{k}'\xi} + \hat{\Xi}_{\mathbf{k}\xi}^\dagger \Gamma_{\mathbf{k}\mathbf{k}'}^{(2)} \hat{\Xi}_{\mathbf{k}'\xi}^\dagger \right) + \text{H.c.}$$

We introduce averaged coupling constants

$$\bar{\Gamma}_{1,2} = \int \frac{d^2\mathbf{k}}{\pi q_0^2} \frac{d^2\mathbf{k}'}{\pi q_0^2} \Gamma_{\mathbf{k}\mathbf{k}'}, \quad (37)$$

where integration is performed over $|\mathbf{k}|, |\mathbf{k}'| < q_0$. The averaged coupling constants $\bar{\Gamma}_{1,2}$ were estimated in Ref. 35, where they were denoted as $\bar{V}_{\text{dir,um}}$. We will use for estimates the values obtained in Ref. 35:

$$\bar{\Gamma}_1 = 9.37t, \quad \bar{\Gamma}_2 = 8.93t. \quad (38)$$

Using these constants, we simplify the interaction Hamiltonian

$$\tilde{H}_{\text{int}}^{\xi} = \frac{-1}{2N_c} \sum_{\mathbf{k}\mathbf{k}'} \text{Tr} \left[2\bar{\Gamma}_1 \hat{\Xi}_{\mathbf{k}\xi}^\dagger \hat{\Xi}_{\mathbf{k}'\xi} + \bar{\Gamma}_2 \left(\hat{\Xi}_{\mathbf{k}\xi}^\dagger \hat{\Xi}_{\mathbf{k}'\xi}^\dagger + \hat{\Xi}_{\mathbf{k}\xi} \hat{\Xi}_{\mathbf{k}'\xi} \right) \right].$$

According to Eq. (16), we have

$$\rho_{10} - \rho_{20} = - \sum_{\mathbf{k}\xi} \text{Tr} \left(\hat{\Xi}_{\mathbf{k}\xi} + \hat{\Xi}_{\mathbf{k}\xi}^\dagger \right). \quad (39)$$

Then, we can express $H_{\text{int}}^{\text{cap}}$ in terms of $\hat{\Xi}$ as

$$\begin{aligned} H_{\text{int}}^{\text{cap}} = & -2\mathcal{E}_0 N_c + \\ & \frac{\mathcal{E}_0}{8N_c} \sum_{\mathbf{k}\mathbf{k}'\xi\xi'} \text{Tr} \left(\hat{\Xi}_{\mathbf{k}\xi} + \hat{\Xi}_{\mathbf{k}\xi}^\dagger \right) \text{Tr} \left(\hat{\Xi}_{\mathbf{k}'\xi'} + \hat{\Xi}_{\mathbf{k}'\xi'}^\dagger \right). \end{aligned} \quad (40)$$

Collecting all these terms, we write the interaction Hamiltonian in the form

$$\begin{aligned} H_{\text{int}} = & \frac{\mathcal{E}_0}{8N_c} \sum_{\mathbf{k}\mathbf{k}'\xi\xi'} \text{Tr} \left(\hat{\Xi}_{\mathbf{k}\xi} + \hat{\Xi}_{\mathbf{k}\xi}^\dagger \right) \text{Tr} \left(\hat{\Xi}_{\mathbf{k}'\xi'} + \hat{\Xi}_{\mathbf{k}'\xi'}^\dagger \right) \\ & - \frac{1}{2N_c} \sum_{\mathbf{k}\mathbf{k}'} \text{Tr} \left[2\bar{\Gamma}_1 \hat{\Xi}_{\mathbf{k}\xi}^\dagger \hat{\Xi}_{\mathbf{k}'\xi} + \bar{\Gamma}_2 \left(\hat{\Xi}_{\mathbf{k}\xi}^\dagger \hat{\Xi}_{\mathbf{k}'\xi}^\dagger + \hat{\Xi}_{\mathbf{k}\xi} \hat{\Xi}_{\mathbf{k}'\xi} \right) \right]. \end{aligned} \quad (41)$$

Here, the c -number contribution $-2\mathcal{E}_0 N_c$ is ignored.

The transformation group G introduced by Eqs. (19) and (20) keeps the interaction Hamiltonian invariant. Such an invariance is a consequence of two features: (i) operator \hat{H}_{int} splits into two valley-specific terms \hat{H}_{int}^ξ , each being invariant under spin rotation \hat{U}_ξ , and (ii) operator $H_{\text{int}}^{\text{cap}}$ depends on the electrical polarization $(\rho_{10} - \rho_{20})$ only, which is a true scalar under the action of the spin rotations in either valleys, as Eq. (39) readily demonstrates.

III. VARIATION VERSION OF THE MEAN FIELD THEORY

A. Mean field variational wave function

Our ultimate goal is to map phase diagram of the many-body model formulated in the previous section. Theoretical tool we use is a zero temperature mean field approach. It is well-known that the mean field method can be implemented using several (equivalent) frameworks: for example, one can view it through lens of the Hubbard-Stratonovich decoupling, or, alternatively, as a self-consistency scheme. Here, we choose variational formulation of the mean field approximation for it allows a consistent treatment of multiple competing ordered phases.

In the mean-field approach the main object is an order parameter. Here we consider exciton-type (non-superconducting) order parameters that open insulating gap. For AB-BLG, such order parameters can be organized into 2×2 matrices $\hat{\Delta}_\xi$ and $\hat{\Delta}_{\bar{\xi}}$, acting in spin space, with the valley labels ξ and $\bar{\xi}$, respectively (bar over index invert its value, $\bar{\xi} = -\xi$). We denote the variational wave function $|\hat{\Delta}_\xi\rangle$ that depends on the proper order parameter.

To construct the desired variational wave function, consider the following Hamiltonian

$$H_{\text{MF}} = H_0 - \sum_{\mathbf{k}\xi} \text{Tr} \left(\hat{\Delta}_\xi \hat{\Xi}_{\mathbf{k}\xi}^\dagger + \hat{\Xi}_{\mathbf{k}\xi} \hat{\Delta}_\xi^\dagger \right). \quad (42)$$

Its ground state $|\hat{\Delta}_\xi\rangle$ satisfies

$$H_{\text{MF}} |\hat{\Delta}_\xi\rangle = E_{\text{MF}} |\hat{\Delta}_\xi\rangle. \quad (43)$$

Here $E_{\text{MF}} = E_{\text{MF}}(\hat{\Delta}_\xi)$ is the ground state energy of $\hat{H}_{\text{MF}}(\hat{\Delta}_\xi)$. Obviously $E_{\text{MF}} = \langle \hat{H}_{\text{MF}} \rangle$, where $\langle \dots \rangle$ denotes averaging with respect to the wave function $|\hat{\Delta}_\xi\rangle$. We use $|\hat{\Delta}_\xi\rangle$ as variational wave function, with $\hat{\Delta}_\xi$ as variational parameter: we vary $\hat{\Delta}_\xi$ to minimize variational energy

$$E_{\text{var}} = \langle H_0 + H_{\text{int}} \rangle. \quad (44)$$

The considered mean field Hamiltonian changes under spin rotation and we can use H_{MF} to describe states with broken spin-rotation symmetry. Group G is broader than the uniform spin-rotation group $U(2)$, therefore, the mean field Hamiltonian changes under the action of G . However, it is easy to see that the Bogolyubov transformation (20) induces a unitary transformation of H_{MF} that can be viewed as a unitary rotation of the order parameter belonging to G . Consequently, the function $E_{\text{MF}} = E_{\text{MF}}(\hat{\Delta}_\xi)$ is invariant under the transformation G , since any eigenenergy remains invariant under a unitary transformation of a Hamiltonian.

The value E_{MF} is not the same as the variation energy E_{var} . However, E_{MF} is a useful technical object for further considerations. The utility of E_{MF} stems specifically from the fact that

$$\sum_{\mathbf{k}} \langle \hat{\Xi}_{\mathbf{k}\xi}^\dagger \rangle = -\frac{\partial E_{\text{MF}}}{\partial \hat{\Delta}_\xi}, \quad (45)$$

as Hellmann-Feynman theorem guarantees. In this formula, the differentiation is performed over matrix elements $[\hat{\Delta}_\xi]_{\sigma\sigma'}$. The indices σ and σ' run from 1 to 2, enumerating all four matrix elements of the 2×2 order parameter matrix.

To perform such a differentiation, one needs to determine how E_{MF} depends on $\hat{\Delta}_\xi$. To find the desired expression, negative eigenvalues of the 4×4 matrix

$$\mathcal{H}_{\mathbf{k}\xi}^{\text{MF}} = \begin{pmatrix} -\varepsilon_{\mathbf{k}} & -\hat{\Delta}_\xi \\ -\hat{\Delta}_\xi^\dagger & \varepsilon_{\mathbf{k}} \end{pmatrix} \quad (46)$$

must be found. Introducing spinors a_i and b_i , we write the following relation for eigenvalues $\varepsilon_{i\xi}$

$$\begin{pmatrix} -\varepsilon_{\mathbf{k}} & -\hat{\Delta}_\xi \\ -\hat{\Delta}_\xi^\dagger & \varepsilon_{\mathbf{k}} \end{pmatrix} \begin{pmatrix} a_i \\ b_i \end{pmatrix} = \varepsilon_{i\xi} \begin{pmatrix} a_i \\ b_i \end{pmatrix}. \quad (47)$$

Therefore,

$$(\varepsilon_{i\xi}^2 - \varepsilon_{\mathbf{k}}^2) a_i = \hat{\Delta}_\xi \hat{\Delta}_\xi^\dagger a_i. \quad (48)$$

This reduces the 4×4 eigenvalue problem to 2×2 one: we need to diagonalize the Hermitian matrix $\hat{\Delta}_\xi \hat{\Delta}_\xi^\dagger$. Once its eigenvalues $\mathcal{D}_{1\xi} \geq 0$, $\mathcal{D}_{2\xi} \geq 0$ are known, the eigenvalues $\varepsilon_{i\xi}$ can be determined according to

$$\varepsilon_{i\xi} = \pm \sqrt{\varepsilon_{\mathbf{k}}^2 + \mathcal{D}_{1,2\xi}}. \quad (49)$$

Now, we can express the ground state energy as a sum of negative $\varepsilon_{i\xi}$

$$E_{\text{MF}} = - \sum_{\mathbf{k}\xi} \left(\sqrt{\varepsilon_{\mathbf{k}}^2 + \mathcal{D}_{1\xi}} + \sqrt{\varepsilon_{\mathbf{k}}^2 + \mathcal{D}_{2\xi}} \right). \quad (50)$$

Since $\sqrt{\varepsilon_{\mathbf{k}}^2 + \mathcal{D}_{1\xi}} + \sqrt{\varepsilon_{\mathbf{k}}^2 + \mathcal{D}_{2\xi}} = \text{Tr} \sqrt{\varepsilon_{\mathbf{k}}^2 + \hat{\Delta}_\xi \hat{\Delta}_\xi^\dagger}$, we can evaluate E_{MF} without diagonalization of $\hat{\Delta}_\xi \hat{\Delta}_\xi^\dagger$:

$$E_{\text{MF}} = - \sum_{\mathbf{k}\xi} \text{Tr} \sqrt{\varepsilon_{\mathbf{k}}^2 + \hat{\Delta}_\xi \hat{\Delta}_\xi^\dagger}. \quad (51)$$

As discussed above, this expression is invariant under unitary transformations of $\hat{\Delta}_\xi$.

Applying Eq. (45) to this formula for E_{MF} , we derive

$$\sum_{\mathbf{k}} \langle \hat{\Xi}_{\mathbf{k}\xi} \rangle = \frac{1}{2} \sum_{\mathbf{k}} \frac{1}{\sqrt{\varepsilon_{\mathbf{k}}^2 + \hat{\Delta}_\xi^\dagger \hat{\Delta}_\xi}} \hat{\Delta}_\xi, \quad (52)$$

connecting the order parameters with anomalous expectation values.

Let us assume that the order parameter is Hermitian, $\hat{\Delta}_\xi^\dagger = \hat{\Delta}_\xi$. In principle, the order parameter needs not be Hermitian: a very general self-consistency condition, derived in Appendix B, admits both Hermitian and non-Hermitian solutions. However, the discussion in Refs. 35 and 36 indicate that non-Hermitian (current-carrying) order parameters are energetically less favorable under realistic conditions. Restricting the analysis to Hermitian matrices therefore represents a substantial simplification of the calculations, while remaining well justified physically.

Hermitian $\hat{\Delta}_\xi$ is diagonalizable

$$\hat{\Delta}_\xi = \hat{U}_\xi \text{diag} (D_{\uparrow\xi}, D_{\downarrow\xi}) \hat{U}_\xi^\dagger, \quad \hat{U}_\xi \in \text{U}(2), \quad D_{\sigma\xi} \in \mathbb{R}. \quad (53)$$

This allows us to derive

$$\sum_{\mathbf{k}} \langle \hat{\Xi}_{\mathbf{k}\xi} \rangle = \sum_{\mathbf{k}} \langle \hat{\Xi}_{\mathbf{k}\xi}^\dagger \rangle = \frac{N_c \nu_0}{2} \hat{U}_\xi \text{diag} \left[D_{\uparrow\xi} \ln \left(\frac{2t_0}{|D_{\uparrow\xi}|} \right), D_{\downarrow\xi} \ln \left(\frac{2t_0}{|D_{\downarrow\xi}|} \right) \right] \hat{U}_\xi^\dagger, \quad (54)$$

where $\nu_0 = t_0/2\sqrt{3}\pi t^2$ is the density of states of undoped

AB-BLG, and $D_{\sigma\xi} \ll t_0$ is assumed. The details of the derivation can be found in Appendix A.

For Hermitian order parameter $\hat{\Delta}_\xi$, the energy E_{MF} is equal to

$$E_{\text{MF}} = - \sum_{\mathbf{k}m} \sqrt{\varepsilon_{\mathbf{k}}^2 + D_m^2}. \quad (55)$$

Here multi-index $m = (\sigma, \xi)$ is introduced: it enumerates four fermion sectors. Mathematically, $D_m = D_{\sigma\xi}$ are (real) eigenvalues of $\hat{\Delta}_\xi$, two eigenvalues, $D_{\uparrow\xi}$ and $D_{\downarrow\xi}$, per each valley. Physically, $|D_m|$ represent four single-electron gaps in four fermion sectors of AB-BLG.

The latter expression for E_{MF} implies that this energy depends only on the Hermitian order parameters' eigenvalues, and is independent of eigenvectors. The sum over \mathbf{k} in Eq. (55) is calculated in Appendix A. Namely,

$$E_{\text{MF}} = E_{\text{MF}}(0) - \frac{1}{2} N_c \sum_m \nu_0 D_m^2 \left[\ln \left(\frac{2t_0}{|D_m|} \right) + \frac{1}{2} \right], \quad (56)$$

where $E_{\text{MF}}(0)$ is a constant independent of the order parameters.

B. Variation energy

Here we evaluate the variation energy (44) as a function of $\hat{\Delta}_\xi$. We can write using Eq. (42)

$$E_{\text{var}} = E_{\text{MF}} + \sum_{\mathbf{k}\xi} \text{Tr} \left(\hat{\Delta}_\xi \langle \hat{\Xi}_{\mathbf{k}\xi}^\dagger \rangle + \langle \hat{\Xi}_{\mathbf{k}\xi} \rangle \hat{\Delta}_\xi^\dagger \right) + \langle H_{\text{int}} \rangle. \quad (57)$$

To calculate $\langle H_{\text{int}} \rangle$, Eq. (41), we apply the Wick theorem and obtain

$$\langle H_{\text{int}} \rangle = \frac{\mathcal{E}_0}{8N_c} \left(\sum_{\mathbf{k}\xi} \text{Tr} \langle \hat{\Xi}_{\mathbf{k}\xi} \rangle + \text{Tr} \langle \hat{\Xi}_{\mathbf{k}\xi}^\dagger \rangle \right)^2 - \frac{1}{2N_c} \sum_{\mathbf{k}\mathbf{k}'\xi} \text{Tr} \left[2\bar{\Gamma}_1 \langle \hat{\Xi}_{\mathbf{k}\xi}^\dagger \rangle \langle \hat{\Xi}_{\mathbf{k}'\xi} \rangle + \bar{\Gamma}_2 \left(\langle \hat{\Xi}_{\mathbf{k}\xi}^\dagger \rangle \langle \hat{\Xi}_{\mathbf{k}'\xi}^\dagger \rangle + \langle \hat{\Xi}_{\mathbf{k}\xi} \rangle \langle \hat{\Xi}_{\mathbf{k}'\xi} \rangle \right) \right]. \quad (58)$$

Therefore, the full expression for the variation energy reads as

$$\begin{aligned} E_{\text{var}}(\hat{\Delta}_\xi) &= E_{\text{MF}} + \sum_{\mathbf{k}\xi} \text{Tr} \left(\hat{\Delta}_\xi \langle \hat{\Xi}_{\mathbf{k}\xi}^\dagger \rangle + \langle \hat{\Xi}_{\mathbf{k}\xi} \rangle \hat{\Delta}_\xi^\dagger \right) - \frac{1}{2N_c} \sum_{\mathbf{k}\mathbf{k}'\xi} \text{Tr} \left[2\bar{\Gamma}_1 \langle \hat{\Xi}_{\mathbf{k}\xi}^\dagger \rangle \langle \hat{\Xi}_{\mathbf{k}'\xi} \rangle + \bar{\Gamma}_2 \left(\langle \hat{\Xi}_{\mathbf{k}\xi}^\dagger \rangle \langle \hat{\Xi}_{\mathbf{k}'\xi}^\dagger \rangle + \langle \hat{\Xi}_{\mathbf{k}\xi} \rangle \langle \hat{\Xi}_{\mathbf{k}'\xi} \rangle \right) \right] \\ &\quad + \frac{\mathcal{E}_0}{8N_c} \left(\sum_{\mathbf{k}\xi} \text{Tr} \langle \hat{\Xi}_{\mathbf{k}\xi} \rangle + \text{Tr} \langle \hat{\Xi}_{\mathbf{k}\xi}^\dagger \rangle \right)^2. \end{aligned} \quad (59)$$

For Hermitian order parameter, we perform summation over \mathbf{k} in Eq. (59) similar to Eq. (56) and obtain

$$\frac{E_{\text{var}}}{N_c} = \frac{E_{\text{MF}}(0)}{N_c} + \frac{\nu_0}{2} \sum_m D_m^2 \left[\ln \left(\frac{2t_0}{|D_m|} \right) - \frac{1}{2} - \frac{\nu_0(\bar{\Gamma}_1 + \bar{\Gamma}_2)}{4} \ln^2 \left(\frac{2t_0}{|D_m|} \right) \right] + \frac{\mathcal{E}_0}{8} \left[\sum_m \nu_0 D_m \ln \left(\frac{2t_0}{|D_m|} \right) \right]^2. \quad (60)$$

In this formula, the last term is the contribution due to

capacitance electrostatic energy, the term proportional

to $(\bar{\Gamma}_1 + \bar{\Gamma}_2)$ corresponds to $\langle \tilde{H}_{\text{int}} \rangle$. The remaining terms come from $\langle H_0 \rangle$.

Analyzing Eq. (60), one can notice that the exchange interaction energy $\langle \tilde{H}_{\text{int}} \rangle$ is non-zero as long as at least one $D_m \neq 0$. At the same time, the electrostatic energy can be nullified even when all D_m 's are finite. This suggests that the system can maintain symmetry broken state even at finite (and, possibly, large) \mathcal{E}_0 energy.

At the same time, the electrostatic charging effects do affect the ordering, as we will see below. Fortunately, we can control, to some extent, these effects by applied bias voltage $e\Phi$. It contributes the following term to the variational energy

$$\delta E_{\text{var}} = \frac{e\Phi}{2} \langle \rho_{10} - \rho_{20} \rangle = -\frac{e\Phi}{2} \sum_{\mathbf{k}\xi} \text{Tr} \left(\hat{\Xi}_{\mathbf{k}\xi} + \hat{\Xi}_{\mathbf{k}\xi}^\dagger \right), \quad (61)$$

where Eq. (39) was used. Expressing traces of the order parameter matrices in terms of D_m 's, see Eq. (54), it is possible to demonstrate that

$$\frac{\delta E_{\text{var}}}{N_c} = -e\Phi P, \quad (62)$$

where

$$P = -\frac{1}{N_c e} \frac{\partial E_{\text{var}}}{\partial \Phi} = \frac{1}{2} \sum_m \nu_0 D_m \ln \left(\frac{2t_0}{|D_m|} \right) \quad (63)$$

is transverse (inter-layer) polarization. Once δE_{var} is added to the right-hand side of Eq. (60), our variational energy is complete.

C. Self-consistency equations

The self-consistency equation can be obtained in general case by minimization of the variational energy (59) over the order parameters $\hat{\Delta}_\xi$. However, such a procedure is quite cumbersome and we placed it in the Appendix B. Here we limit ourselves to the case of the Hermitian order parameters. Therefore, our task here is to minimize the energy, expressed by Eqs. (60) and (62), over D_m 's. Differentiating over D_m , we obtain

$$\frac{\nu_0}{2} D_m \ln \left(\frac{2t_0}{|D_m|} \right) = \frac{D_m}{\bar{\Gamma}_1 + \bar{\Gamma}_2} - \quad (64)$$

$$\frac{\mathcal{E}_0}{2(\bar{\Gamma}_1 + \bar{\Gamma}_2)(2\mathcal{E}_0 - \bar{\Gamma}_1 - \bar{\Gamma}_2)} \sum_{m'} D_{m'} + \frac{e\Phi}{2(2\mathcal{E}_0 - \bar{\Gamma}_1 - \bar{\Gamma}_2)}.$$

Our Eqs. (28) and (38) allow us to establish the following inequality

$$2\mathcal{E}_0 > (\bar{\Gamma}_1 + \bar{\Gamma}_2). \quad (65)$$

It implies that all material-specific coefficients in Eq. (64) are positive. Our analysis will be mostly focused on this regime. Yet, inequality (65) is not fundamental and may

be violated. While not identical, these two limits shares a lot of features, as we will see below.

It is convenient to introduce a BCS-like order parameter as

$$\Delta_0 = 2t_0 \exp \left(-\frac{2}{\nu_0(\bar{\Gamma}_1 + \bar{\Gamma}_2)} \right), \quad (66)$$

After a simple algebra we derive the self-consistency equations in the final form

$$D_m \ln \left(\frac{\Delta_0}{|D_m|} \right) = -\frac{\mathcal{E}_0}{\nu_0(\bar{\Gamma}_1 + \bar{\Gamma}_2)(2\mathcal{E}_0 - \bar{\Gamma}_1 - \bar{\Gamma}_2)} \sum_{m'} D_{m'} + \frac{e\Phi}{\nu_0(2\mathcal{E}_0 - \bar{\Gamma}_1 - \bar{\Gamma}_2)}, \quad m = 1, \dots, 4. \quad (67)$$

Here, the multi-index m enumerate all four possible choices of the spin $\sigma = \uparrow\downarrow$, and valley $\xi = \pm 1$. From the formal mathematical point of view, the exact order of this enumeration does not affect the solution of this set of equations. However, choosing different order of enumeration we will obtain different physical phases.

Expression (67) is the central result of the paper. Together with the variational energy formulas, it allows us to analyze the mean-field phases of biased AB-BLG.

IV. MEAN FIELD PHASES

A. Ferroelectric state

First we discuss the simple ferroelectric (FE) state in the AB-BLG. Namely, we assess the possibility of spontaneous inter-layer polarization of AB-BLG at $e\Phi = 0$. This question caused some controversy back in early days of bilayer research: Ref. 16 argued that, unless external electric field is applied, the FE phase stability is destroyed by large electrostatic energy cost, which was challenged in Ref. 17, where it was proposed that the contributions due to exchange interaction \tilde{H}_{int} is sufficient to overcome the electrostatic energy, and the FE phase can become stable. Our calculations presented below demonstrate that for realistic conditions the FE state is likely to be unstable.

We begin our investigation with the observation that in the FE phase all four D_m 's have identical absolute values and identical signs. That is

$$D_m = D_{\text{FE}} \quad \text{for all } m. \quad (68)$$

Using $\sum_{m'} D_{m'} = 4D_{\text{FE}}$ in Eqs. (64), one can derive an equation for D_{FE}

$$D_{\text{FE}} \left[\lambda_{\text{FE}} \ln \left(\frac{2t_0}{|D_{\text{FE}}|} \right) + 1 \right] = \frac{e\Phi}{2}, \quad (69)$$

$$\lambda_{\text{FE}} = \frac{\nu_0(2\mathcal{E}_0 - \bar{\Gamma}_1 - \bar{\Gamma}_2)}{2} \approx 0.461.$$

When no bias voltage is applied, we have

$$\ln\left(\frac{2t_0}{|D_{\text{FE}}|}\right) = -\frac{1}{\lambda_{\text{FE}}}. \quad (70)$$

This equation has formal solution $|D_{\text{FE}}| = \mathfrak{E}$, where the energy scale

$$\mathfrak{E} = 2t_0 e^{1/\lambda_{\text{FE}}} \quad (71)$$

is introduced. Yet this root $\mathfrak{E} \approx 7 \text{ eV}$ violates the condition $|D_{\text{FE}}| < 2t_0$ for our two-band model. One must conclude that, unless bias field is applied, only trivial solution $D_{\text{FE}} = 0$ for Eq. (69) is valid, in agreement with results of Ref. 16.

What would happen when the external field is applied? In the limit of high bias voltage when we can neglect interaction, Eq. (69) has an obvious solution $D_{\text{FE}} = e\Phi/2$. That is, the application of the bias voltage opens a gap in the spectrum proportional to the electric field. This case corresponds to the limit $\lambda_{\text{FE}} \ln(4t_0/e\Phi) \ll 1$, or, equivalently,

$$\frac{e\Phi}{2} \gg \mathfrak{E} > 2t_0. \quad (72)$$

Inequality (72) is inconsistent with the two-band applicability criterion (10). Additionally, for relation (72) to be valid, the electric field between graphene layers must be at least $2\mathfrak{E}/d \approx 4 \times 10^8 \text{ V/cm}$, which is quite large.

At smaller fields, the interaction effects cannot be ignored. It is useful to rewrite Eq. (69) in the form

$$\frac{D_{\text{FE}}}{\mathfrak{E}} \ln\left(\frac{\mathfrak{E}}{|D_{\text{FE}}|}\right) = \frac{e\Phi}{2\lambda_{\text{FE}}\mathfrak{E}}. \quad (73)$$

Thus, we need to analyze the equation

$$x \ln\left(\frac{1}{|x|}\right) = y, \quad (74)$$

in the limit $|y| \ll 1$, where $x = D_{\text{FE}}/\mathfrak{E}$ and $y = e\Phi/(2\lambda_{\text{FE}}\mathfrak{E})$. The dependence $x = x(y)$ can be learned from the plot in Fig. 1. There we observe three branches of the function $y = y(x)$: the first starts from $x = 0$, the second and third branches pass through $x = \pm 1$. The branches merge at $|x| = y = 1/e$. It is evident that only the first one is physical and obeys the condition $|y| \ll 1$. The first branch corresponds to the required FE state induced by the gate voltage. As one might expect, the gap D_{FE} grows monotonically when the voltage grows.

We can see that, for $|y| > 1/e$, there is no solution of Eq. (74) on the physical branch. One can speculate, if this implies that at $|y| = 1/e$ an electric breakdown of the bilayer occurs. However, we must remember that our model is valid only in the regime $e\Phi/2, |D_m| \ll 2t_0$, which does not cover the fields near the extrema.

We already pointed out that, in our model, no spontaneous FE gap D_{FE} exists. This absence of spontaneous FE order may be traced back to inequality (65). Basically, the inequality tells us that the macroscopic electric

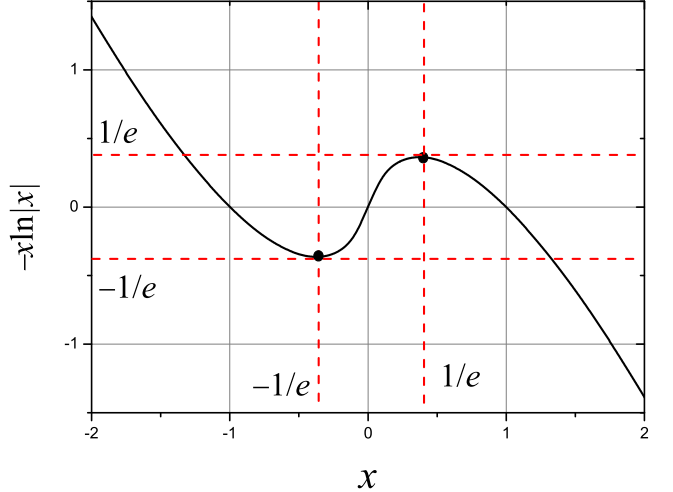


FIG. 1. Function $y = x \ln(1/|x|)$. Formally, the derivative of the function diverges at $x = 0$ as $\sim \ln(1/|x|)$. Yet, due to weakness of this divergence, vertical tangent is essentially unobservable on the plot.

polarization of the sample is very costly in terms of energy (large \mathcal{E}_0), and any potential energy minimization due to exchange contributions (Fock terms) cannot compensate large electrostatic energy.

At the same time, if inequality (65) is violated, λ_{FE} is negative, and the energy scale $\mathfrak{E} = 2t_0 e^{-1/|\lambda_{\text{FE}}|}$ becomes less than $2t_0$. This makes the zero-bias FE solution

$$|D_{\text{FE}}| = \mathfrak{E} = \Delta_0 \exp\left[-\frac{2\mathcal{E}_0}{|\lambda_{\text{FE}}|(\bar{\Gamma}_1 + \bar{\Gamma}_2)}\right] \quad (75)$$

compatible with the two-band model assumption $|D_{\text{FE}}| < 2t_0$, in agreement with Ref. 17. It is easy to check that, as long as \mathcal{E}_0 remains finite, one has $|D_{\text{FE}}| < \Delta_0$. Thus, violation of (65) turns the FE phase metastable at $e\Phi = 0$. However, the FE cannot become zero-bias ground state as solutions with zero spontaneous electrostatic polarization have larger order parameter ($\sim \Delta_0$), and lower energy. It is likely that $\lambda_{\text{FE}} < 0$ regime was modeled numerically in Ref. 22.

B. Layered antiferromagnetic and other possible states

Large positive contribution due to the electrostatic energy, which destabilized the FE phase, can be drastically reduced if the FE phase requirement (68) is abandoned, and D_m 's are allowed to vary from one fermion sector to another. Such a situation corresponds to several orderings, including, in particular, the layered antiferromagnetic state, as well as other phases with non-zero spin or valley polarization. To describe them, it is convenient to

re-write the set of equations (67) as follows

$$\begin{aligned} \left(\frac{D_m}{\Delta_0}\right) \ln\left(\frac{\Delta_0}{|D_m|}\right) &= \frac{e\Phi}{2\lambda_{\text{FE}}\Delta_0} - \\ \frac{\mathcal{E}_0}{2\lambda_{\text{FE}}(\bar{\Gamma}_1 + \bar{\Gamma}_2)} \sum_{m'} \left(\frac{D_{m'}}{\Delta_0}\right), \quad \text{for } m=1, \dots, 4. \end{aligned} \quad (76)$$

To solve this set of equations, let us introduce dimensionless constant $\Lambda = \mathcal{E}_0/[2\lambda_{\text{FE}}(\bar{\Gamma}_1 + \bar{\Gamma}_2)]$. It can be equivalently expressed as

$$\Lambda = \frac{\mathcal{E}_0}{\nu_0(2\mathcal{E}_0 - \bar{\Gamma}_1 - \bar{\Gamma}_2)(\bar{\Gamma}_1 + \bar{\Gamma}_2)} \approx 2.55. \quad (77)$$

This is a very important parameter that controls various physical properties of AB-BLG. It satisfies

$$\frac{1}{2\gamma} < \Lambda, \quad \text{where } \gamma = (\bar{\Gamma}_1 + \bar{\Gamma}_2)\nu_0 \approx 0.249. \quad (78)$$

Clearly, our estimate (77) is consistent with inequality (78). It is also worth keeping in mind that, for the mean field to be valid, $\gamma/2$ must be smaller than unity. Consequently, $\Lambda > 1/(2\gamma) > 0.25$, which may be viewed as the lowest possible bound on Λ .

We further define dimensionless applied voltage V and dimensionless gap parameters x_m according to

$$x_m = \frac{D_m}{\Delta_0}, \quad V = \frac{e\Phi}{2\lambda_{\text{FE}}\Delta_0}. \quad (79)$$

Using these notations, we rewrite Eq. (76) as

$$x_m \ln\left(\frac{1}{|x_m|}\right) = V - \Lambda(x_1 + x_2 + x_3 + x_4). \quad (80)$$

Here all variables x_m can be either positive, or negative, or zero. From the physical point of view, the term proportional to Λ in Eq. (80) describes the suppression of the inter-layer charge polarization due to significant electrostatic energy. If the applied potential V is zero, this energy contribution is the smallest at $\sum_{m'} x_{m'} = 0$. A finite applied potential V shifts this minimum from zero of $\sum_{m'} x_{m'}$ to non-zero value.

The system of Eqs. (80) includes four unknowns. Mathematical search for its roots is greatly simplified due to the following feature: all four equations have identical right-hand side, which is independent of m . Thus, for any $m \neq m'$

$$x_m \ln\left(\frac{1}{|x_m|}\right) = x_{m'} \ln\left(\frac{1}{|x_{m'}|}\right). \quad (81)$$

An evident solution of the latter equation is $x_m = x_{m'}$. Yet, this is not the only possibility. We already discussed function $y(x) = x \ln(1/|x|)$ in connection with solutions of Eq. (74), see Fig. 1: clearly, the equation

$$x \ln\left(\frac{1}{|x|}\right) = C, \quad (82)$$

may have one, two, or three roots, depending on $|C|$. It is convenient to denote the three possible solutions of Eq. (82) as x_{\pm} and x_s according to the following rule:

$$x_- < -1/e, \quad x_+ > 1/e, \quad -1/e < x_s < 1/e, \quad (83)$$

one root per branch of $y(x)$. With this definition, the set of equations (80) can be reformulated in a parametric representation

$$V = C + \Lambda [n_s x_s(C) + n_+ x_+(C) + n_- x_-(C)], \quad (84)$$

where $x_{\pm} = x_{\pm}(C)$ and $x_s = x_s(C)$ satisfy Eq. (82) and inequalities (83). Non-negative integers $0 \leq n_{\pm} \leq 4$, $0 \leq n_s \leq 4$ satisfy the relation

$$n_+ + n_- + n_s = 4. \quad (85)$$

The integer n_s (integer n_{\pm}) show how many roots x_s (roots x_{\pm}) among four variables $x_{1, \dots, 4}$.

There are 15 possible partitions of four into three parts. This specifies 15 solutions of Eq. (80), one solution for a given partition. For example, the FE state corresponds to $n_s = 4$, $n_{\pm} = 0$. It is easy to check that the layered antiferromagnet is represented by the choice $n_s = 0$, $n_{\pm} = 2$. This guarantees that electrostatic effects represented by $\Lambda \sum_{m'} x_{m'}$ are small in the layered antiferromagnet state: in this sum, two terms are positive and two terms are negative. However, among these solutions some are physically equivalent. For example, the transition between phases with $n_s = 4$, $n_{\pm} = 0$ and $n_s = 0$, $n_- = 0$, $n_+ = 4$, occurs at some $V = 4.122$ (for $\Lambda = 2.55$) without any thermodynamic changes and is not a phase transition. In addition, the system properties are evidently symmetric with respect to the sign of the applied voltage. Thus, in what follows we consider only the case of $V > 0$.

C. Ordered state energy

Among these solutions, a single ground state must be identified for every V . To find the ground state, we need to calculate the variational energies of the competing phases, and compare them against each other. To this end, we re-write the variational energy (60) and (62) in the form

$$\begin{aligned} \bar{E} &= \frac{1}{2} \sum_m x_m^2 \left[\ln\left(\frac{1}{\delta_0|x_m|}\right) - \frac{\gamma}{2} \ln^2\left(\frac{1}{\delta_0|x_m|}\right) - \frac{1}{2} \right] + \\ &\quad \frac{\bar{\varepsilon}}{8} \left[\sum_m x_m \ln\left(\frac{1}{\delta_0|x_m|}\right) \right]^2 - V \lambda_{\text{FE}} \sum_m x_m \ln\left(\frac{1}{\delta_0|x_m|}\right), \end{aligned} \quad (86)$$

where

$$\bar{E} = \frac{E_{\text{var}} - E_{\text{MF}}(0)}{N_c \nu_0 \Delta_0^2}, \quad \delta_0 = \frac{\Delta_0}{2t_0}, \quad (87)$$

$$\bar{\varepsilon} = \mathcal{E}_0 \nu_0 \approx 0.585. \quad (88)$$

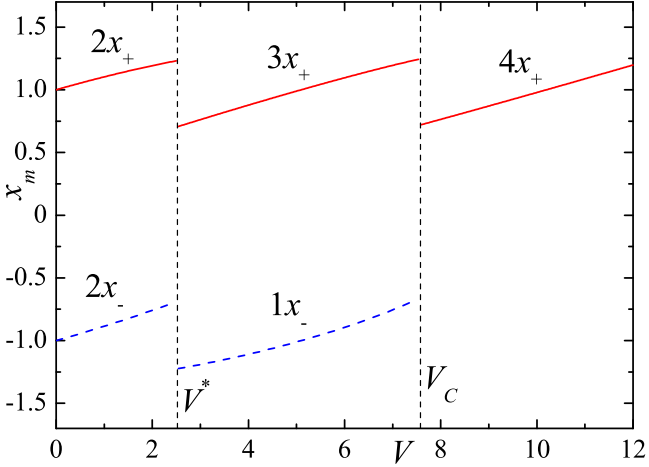


FIG. 2. The phase diagram of the system at $V > 0$ and the dependence of the order parameters $x_m = D_m / \Delta_0$ on the applied voltage (red lines are the solutions x_+ and blue x_-). The voltage $V^* \approx 2.3$ corresponds to the transition between the "antiferromagnetic states" with $(n_+ = 2, n_- = 2)$ and $(n_+ = 3, n_- = 1)$. When $V > V_C \approx 8.8$ the "antiferromagnetic orders" disappear and the gap in the spectrum is due to the layers polarization only.

When x_m 's in Eq. (86) satisfy the self-consistency equations (80), the expression for the system's energy can be simplified: after rather straightforward calculations, one can derive

$$\bar{E} = -\frac{1}{4} \sum_m x_m^2 + \frac{V}{2} \sum_m x_m - 2\lambda_{FE} V^2. \quad (89)$$

The first term in this formula represents the mean field condensation energy, the others are induced by the electrostatic interaction between the external field and the inter-layer polarization.

V. PHASE DIAGRAM

A. General remarks

In our model, the ordered states depend only on two dimensionless parameters, V and Λ . Indeed, of all model parameters, only V and Λ enter the dimensionless self-consistency equations (80). Competition between ordered states is controlled by \bar{E} , the latter being a sum of three terms, of which two (the first and the second terms) depend explicitly on V , and implicitly (through x_m) on V and Λ . One can suggest superficially that λ_{FE} might affect the phase diagram as it enters the third term in Eq. (89). Yet, this contribution is the same for all ordered phases, and, consequently, does not affect their competition at fixed V and Λ . Therefore, we conclude that the values of two dimensionless parameters, V and Λ , determine the ground state order in our model.

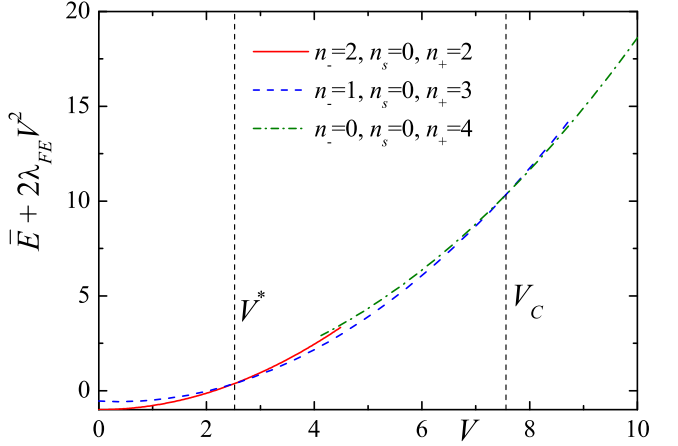


FIG. 3. The system energies as functions of the applied voltage. For $V \geq 0$, only three ground states are possible, see the legend. The plotted energy is the sum of the first and the second terms in definition (89). The third term in Eq. (89), while contributing a large offset to the total energy, does not influence relative stability of phases. It is therefore omitted for clarity. For $V < V^*$, the solid (red) curve is the lowest. Thus, the solution $n_{\pm} = 2$ is the ground state. As V increases, a transition into $n_+ = 3, n_- = 1$ type, followed by the second transition into the FE state $n_+ = 4, n_- = 0$, occurs. Note that in the interval $V^* < V < V_C$ the solution $n_{\pm} = 2$ disappears, while the FE solution emerges. When V exceeds V_C sufficiently, the solution $n_+ = 3, n_- = 1$ disappears, leaving the FE solution the only one at elevated V .

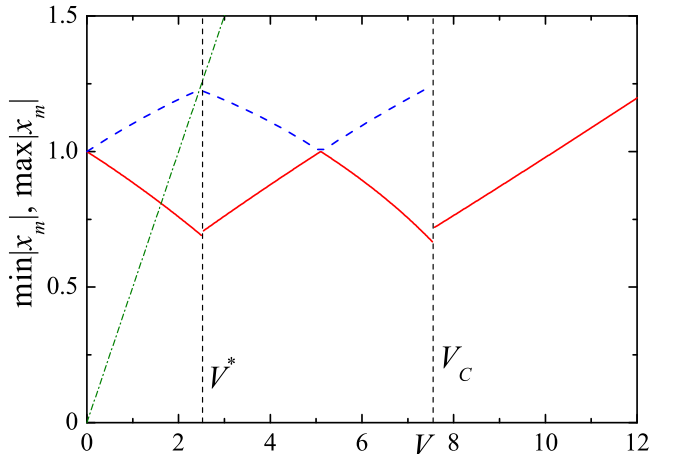


FIG. 4. Dependence of dimensionless single-electron gap $\min_m |x_m|$ (red solid line) versus dimensionless bias V . In the interval $0 < V < V_C$, both $n_{\pm} > 0$, thus, positive and negative x_m 's may have unequal $|x_m|$, see Fig. 2. For such values of V , dashed (blue) line shows $\max_m |x_m|$. The gap is a non-monotonic function of V , with discontinuities at $V = V^*, V_C$. At $V = 2\Lambda$, the gap has local maximum $x = 1$, see Sec. V D. Dash-dotted (green) line is $\Delta = e\Phi/2$, or, in dimensionless units, $x = \lambda_{FE}V$. It represents bias-induced gap in the model with no interaction. We see that interaction effects screen the bare field significantly.

For value of Λ as in Eq. (77), numerically calculated phase diagram is shown in Fig. 2. The figure also presents the dependence of the order parameters on the applied voltage $V > 0$. Figure 3 shows the energies of the states that become ground state at certain V .

We see that, at zero or low bias, the ground state corresponds to the solution $n_+ = n_- = 2$. As V grows, two phase transitions occur. At $V^* \approx 2.51$ the solution $n_+ = n_- = 2$ is replaced by $n_+ = 3, n_- = 1$ solution. The transition occurs when the energies of these solutions, expressed by Eq. (89), become equal each other, see Fig. 3.

As V exceeds $V_C \approx 7.6$, solution $n_+ = 4, n_- = 0$ becomes the ground state. It remains the ground state for even higher voltages, as long as the model remains valid.

To extrapolate Figs. 2 and 3 to $V < 0$, we can use the symmetry of the phase diagram relative to $V = 0$ point: simultaneous substitutions $V \rightleftarrows -V$ and $n_+ \rightleftarrows n_-$ keep the phase diagram unchanged.

For electronic states in sector $m = (\xi, \sigma)$, the value of $|D_m|$ represents the single-electron gap in this fermion sector. Clearly, the overall spectral gap, visible in, e.g., transport experiments, is the smallest of $|D_m|$'s, or, in dimensionless units, $\min_m |x_m|$, see Fig. 4. We see that the gap is non-monotonic function of the bias. For comparison, the latter figure plots the non-interacting model gap $e\Phi/2$. We see that interaction effects reduce this “bare” gap quite dramatically (except low-bias regime, where spontaneous gap exceeds the bare one).

B. Linearized self-consistency equations

Curiously, the phase diagram may be recovered analytically. If we assume that $|x_m|$ is close to unity, we can approximate $x_m \ln(1/|x_m|) = -\zeta_m + O(\zeta_m^2)$ for $x_m = \pm 1 + \zeta_m$. Using Eq. (81), one can conclude that all ζ_m 's are identical for any m . Thus, we can drop subscript and write $\zeta = \zeta_m$. In this approximation, the self-consistency conditions (80) become

$$-\zeta \approx V - \Lambda(n_+ - n_-) - 4\Lambda\zeta, \quad (90)$$

and can be solved

$$\zeta \approx \frac{V - \Lambda(n_+ - n_-)}{4\Lambda - 1}. \quad (91)$$

This solution is valid as long as ζ is small. Also, because of singularity at $x = 0$, linearization is impossible for solutions with $n_s > 0$. Fortunately, our numerical data indicates that we can ignore them, as long as Λ is not too small.

Substituting approximate solutions (91) in formula (89), we derive the following approximate expression

$$\bar{E} \approx -1 - \frac{2\lambda_{\text{FE}}^2}{\bar{\varepsilon}} V^2 + \left(1 - \frac{1}{2\Lambda}\right) \zeta^2. \quad (92)$$

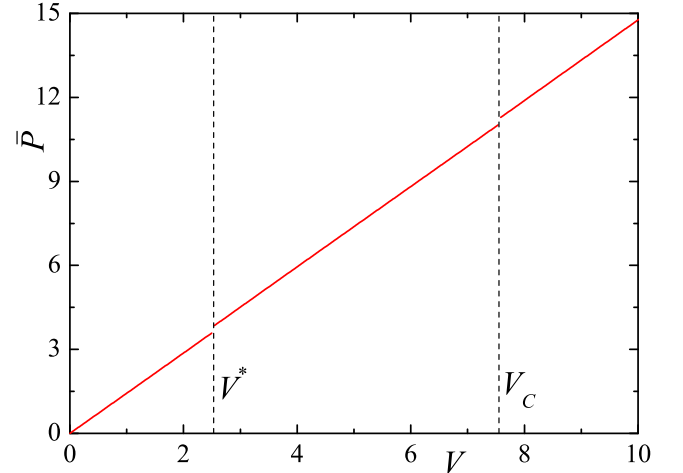


FIG. 5. Numerically estimated dimensionless polarization \bar{P} versus the dimensionless bias voltage V . The plot for \bar{P} demonstrates discontinuities at the transition points $V = V^*$ and $V = V_C$. Between the transitions, the graph is virtually indistinguishable from linear function. This behavior is in agreement with Eq. (96), attesting the quality of approximate solution (91).

This energy depends on the solution type through ζ .

Using the latter formula, we establish $V^* \approx \Lambda$, and $V_C \approx 3\Lambda$. Both estimates are consistent with our numerical results. If $|V|$ does not exceed V_C too much, the value of $|\zeta|$ remains below 0.28, which guarantees good practical accuracy of the linear approximation.

Alternatively, we can write that the transitions between the phases occur at the following bias values

$$e\Phi^* = \frac{\mathcal{E}_0}{\bar{\Gamma}_1 + \bar{\Gamma}_2} \Delta_0, \quad e\Phi_C = \frac{3\mathcal{E}_0}{\bar{\Gamma}_1 + \bar{\Gamma}_2} \Delta_0, \quad (93)$$

where $e\Phi^* = 2\lambda_{\text{FE}}\Delta_0 V^*$, and $e\Phi_C = 2\lambda_{\text{FE}}\Delta_0 V_C$.

Obviously, there is a “universal” connection between $e\Phi^*$ and $e\Phi_C$

$$\frac{e\Phi_C}{e\Phi^*} = 3, \quad (94)$$

which can be used for analysis of experimental or numerical data.

C. Layered antiferromagnet

Both numerical and approximate analytical solutions demonstrate that, for our choice of Λ , in the interval $|V| < V^*$, the solution $n_+ = n_- = 2$ has the lowest energy, see Fig. 3. In this regime, $\zeta = V/(4\Lambda - 1)$.

There are $C_4^2 = 6$ possible assignments of two pluses ($n_+ = 2$) and two minuses ($n_- = 2$) among four x_m 's. These six choices can be grouped into three pairs, each pair representing either layered antiferromagnet (LA), or quantum anomalous Hall (QAH) state, or quantum spin

Hall (QSH) state³⁷. Every pair can be characterized by a certain spontaneous polarization (spin, valley, or spin-valley), which breaks one of the model's symmetries³⁵. States within a pair are connected to each other by inversion of the polarization's sign.

Due to our model's simplifications, all these states have the same energy, and the ground state smoothly evolves as V changes. Yet, it is necessary to remember that a more complicated framework^{23,25,33} can lift this degeneracy: previous calculations indicate^{25,33} that LA is the ground state of AB-BLG at $V = 0$. If the degeneracy is removed, a possibility of first-order transitions between the LA/QAH/QSH states must be kept in mind as small energies separating the latter phases might be voltage-dependent.

Clearly, the applied voltage makes polarization P , introduced by Eq. (63), finite. It is easy to demonstrate that, for x_m satisfying the self-consistency equations (80), dimensionless polarization $\bar{P} = -\partial\bar{E}/\partial V$ is

$$\bar{P} = 4\lambda_{\text{FE}}V - \sum_m x_m. \quad (95)$$

Numerically estimated $\bar{P}(V)$ is plotted in Fig. 5. On the other hand, using approximation (91), one can derive

$$\bar{P} \approx 4 \left(\lambda_{\text{FE}} - \frac{1}{4\Lambda - 1} \right) V + \frac{n_+ - n_-}{4\Lambda - 1}. \quad (96)$$

Substituting $n_+ = n_- = 2$ into this formula, we find $\bar{P} \approx 1.41V$, which agrees well with the data in Fig. 5.

At $V = 0$, we have $|x_m| = 1$ for all m . As V deviates from zero, disparity emerges: if $x_m > 0$, its absolute value $|x_m|$ increases (decreases) for positive (negative) V . For $x_m < 0$, the trend is opposite. This feature has an important consequence. Single-electron gap $E_g(V) = 2\Delta_0 \min_m |x_m(V)|$ becomes a function of voltage, see Fig. 4. In the LA phase, the gap is the largest at $V = 0$. The gap modulation may be detected in transport experiments.

D. Transition at $V = V^*$

When V crosses V^* , the lowest energy solution is $n_+ = 3, n_- = 1$, see Fig 3. Likewise, solution $n_+ = 1, n_- = 3$ becomes the ground state at $V = -V^* < 0$. These solutions are stable in the range $V^* < |V| < V_C$. Thus, condition $|V| = V^*$ marks locations of first-order transitions.

There are $C_4^1 = 4$ possible sign assignments for $n_+ = 3, n_- = 1$ solution. Each assignment represents one of four QAH-type phases, which form a degenerate quartet. Another quartet of symmetry-related QAH phases emerge at $V < -V^*$. In terminology of Ref. 35, these are class III states. When smoothly extrapolated to $V = 0$, all these phases have finite valley, spin, spin-valley, and charge polarizations. Finite charge polarization undermines their

stability at low bias. Yet, at finite V , the same feature improves their stability relative to the LA.

Both \bar{P} and $|x_m|$ exhibit jumps at the transition point, see Fig. 5 and Fig. 2. If we use approximation (96), the polarization discontinuity is controlled by the second term: $n_+ - n_-$ changes by 2 at the transition. Thus, the discontinuity can be estimated as $2/(4\Lambda - 1) \approx 0.22$, in agreement with the numerical calculations.

Beside the discontinuities at the transitions points, the data in Fig. 4 reveals that, at certain bias all $|x_m|$ are identical for both positive and negative x_m . It is easy to check that such a condition can be fulfilled when $|x_m| = 1$ for all m . This further implies that the right-hand side of Eq. (80) vanishes. For $n_+ = 3, n_- = 1$, this is only possible when bias is equal to $V_{\text{max}} = 2\Lambda$, or, equivalently,

$$e\Phi_{\text{max}} = \frac{2\mathcal{E}_0}{\bar{\Gamma}_1 + \bar{\Gamma}_2} \Delta_0. \quad (97)$$

This is exact relation, and not a consequence of approximation (91). A “universal” ratio

$$\frac{e\Phi_{\text{max}}}{e\Phi^*} = 2, \quad (98)$$

on the other hand, is an approximate relation since it relies on Eq. (93), the latter being derived using linearization.

Examining Fig. 4, one can check that the single-electron gap is a non-monotonic function of V within this phase: the maximum gap is $|x_m| = 1$, or, in dimensional units, Δ_0 . This value is reached at $e\Phi = e\Phi_{\text{max}}$.

E. Finite-bias ferroelectric state

When V crosses V_C , solution $n_+ = 4$ becomes the ground state. It is non-degenerate and represents the FE phase. It may also be classified³⁷ as a quantum valley Hall state.

For our Λ estimate, the FE is unstable at zero voltage, yet, it becomes stable when external electric field is applied. As with the QAH phases discussed in subsection V D, finite polarization of the FE phase pushes its energy upward at low bias fields, while at large V it is the most important factor of the FE state stabilization.

The polarization is discontinuous at $V = V_C$, as the numerical data in Fig. 5 attest. Formula (96) shows that the discontinuity is 0.22, the same as the discontinuity at $V = V^*$.

The gap changes discontinuously at the transition, see Fig. 4. Beyond V_C , the gap monotonically increases when $|V|$ grows.

VI. DISCUSSION

A. Comparison with experiment

To compare our results with experiment, we need to determine the zero-bias order parameter size Δ_0 . It is possible to use the definition (66) and evaluate $\Delta_0 \approx 0.27$ meV. This is order of magnitude smaller than the reported^{3,7,10} value of ~ 2 meV. Such a difference between the experiment and theory is not surprising. Due to non-analytical dependence of Δ_0 on $\gamma/2$, even moderate errors in our knowledge of the coupling constant strength may severely skew the value of Δ_0 . Additionally, the pre-exponential energy scale is not immediately known. In the two-band theory we are limited by the pre-exponential being of order of t_0 , which is fairly small energy. As we will see below, in the Hartree-Fock calculations of Ref. 22 the pre-exponential energy is drastically larger than t_0 , leading to unrealistically large values of Δ_0 . In such a situation, it appears more prudent to use order parameter value from experiment. Thus, below we will assume that $\Delta_0 = 2$ meV.

Our theory predicts several features that may be tested against experiment, at least in principle. We know that the bias induces phase transitions between various thermodynamic states of AB-BLG. Also, the field changes the value of single-electron gap: the gap is a non-monotonic function of $e\Phi$. Such behavior have identifiable experimental consequences, as the gap is often affects low-temperature transport measurements. In this regard, let us mention experiment of Ref. 31 that does show non-monotonicity of resistance as a function of bias field, see Fig. 2(b) of the latter paper.

Unfortunately, the measured pattern of resistance versus bias cannot be completely understood within the framework of our theory. Specifically, the variation of the resistance of AB-BLG sample does not trace the variation of the gap in Fig. 4. Yet, partial interpretation of the data is still possible.

On the experimental curve for device A in Ref. 31, one can see a well-defined maximum at zero bias, which may be associated with the gap that our calculations find at $e\Phi = 0$.

Away from the zero-bias state, the resistance data shows symmetric minima at $\sim \pm 20$ mV/nm, which correspond to

$$e\Phi_{\min}^{\text{exper}} \approx \pm 6.7 \text{ meV}. \quad (99)$$

Identifying the minimum of resistance with the gap minimum at $e\Phi^*$, that is, equating $e\Phi^* = e\Phi_{\min}^{\text{exper}}$, and assuming that the low-temperature gap size is $\Delta_0 = 2$ meV, as agreed above, it is possible to evaluate the ratio

$$\left(\frac{\mathcal{E}_0}{\bar{\Gamma}_1 + \bar{\Gamma}_2} \right)_{\text{exper}} \approx 3.4. \quad (100)$$

The latter number is roughly consistent with our theoretical estimate ~ 2.3 , which follows from Eqs. (28)

and (38). Additionally, since Eq. (100) does not violate inequality (65), we conclude that both Λ and λ_{FE} are positive, and the FE state is absolutely unstable at zero bias, as we discussed in Sec. IV A.

Using “universal” relations (94) and (98), it is possible to estimate the maximum gap bias as $e\Phi_{\max}^{\text{exper}} = 2e\Phi_{\min}^{\text{exper}} \approx \pm 13$ meV, which is equivalent to transverse field of ± 40 mV/nm. Further, the theory indicates that, at ± 60 mV/nm, the gap minimum corresponding to $e\Phi_C$ must be visible. Yet, instead of these features, the resistance plot shows a shoulder (or broad maximum) for the field to the left of -30 mV/nm, or, equivalently, for $e\Phi < -10$ meV.

Since no data at high bias $|e\Phi| > 20$ meV were reported, the properties of the high-bias FE state remain untested. Specifically, the expected steady increase of single-electron gap with increasing V beyond V_C is not apparent in the data of Ref. 31.

At the same time, we must remember that the energy differences between the competing phases are very small. Indeed, examining Fig. 3, we see that the competing solutions’ energies differ by less than $\sim \nu_0 \Delta_0^2 = 2 \times 10^{-8}$ eV per unit cell. In addition, both $n_{\pm} = 2$ solution and $n_+ = 3, n_- = 1$ solution each represent several degenerate phases, see discussion in subsections V C and V D.

In this situation, several factors may alter the relative stability of the competing phases and thereby modify the phase diagram. Furthermore, domain walls between degenerate or nearly degenerate states can arise. Because such domain walls may be conducting, transport measurements may constitute an unreliable probe of the single-electron gap.

B. Comparison with Hartree-Fock simulations

While exhaustive comparison with the experiment is challenging at this point, our conclusions agree quite well with extensive numerical Hartree-Fock simulations of AB-BLG, presented in Ref. 22. Specifically, Fig. 5 of Ref. 22 is analogous to Fig. 3 of the present paper. It shows that the low-bias AF phase (our $n_{\pm} = 2$ solution) is replaced by Fi phase (represents our $n_+ = 3, n_- = 1$ solution). The latter is ultimately replaced by F phase (that is, the FE phase in our terminology) at higher external fields. It is easy to check that bias fields at which these transitions occur satisfy “universality” relation (94).

Examining lower panel of Fig. 6 in Ref. 22, we clearly see a gap maximum inside the Fi phase. In terms of the bias, the maximum is located exactly in the middle of the Fi phase, precisely in agreement with relation (98). Note that the gap value at this maximum is exactly the same as zero-bias gap (both are ~ 33 meV). This feature is clearly visible in our Fig. 4, where the gap at $V = 0$ and the gap at $V = 2\Lambda \approx 5.1$ are equal to each other.

It is possible to extract model parameters from the data in Figs. 5 and 6 of Ref. 22. This is described in

detail in Appendix C. We would like to draw attention of a reader to two circumstances. (i) It is demonstrated that the Hartree-Fock data corresponds to the regime of negative λ_{FE} and Λ . This means that inequality (65) is violated. We already commented above that this inequality is not of the fundamental nature. However, both our estimates and experimental data in Ref. 31 indicate that relation (65) does hold true. For some unclear reason, the Hartree-Fock simulation underestimates \mathcal{E}_0 energy (finite dielectric constant assumed for the simulations is not large enough to account for the discrepancy). Smallness of \mathcal{E}_0 relative to $\tilde{\Gamma}_{1,2}$ makes the FE phase metastable at $e\Phi = 0$, which indeed what Ref. 22 reported, see Fig. 5 there.

Additionally, (ii) the order parameters values in Ref. 22 are very large: 16 meV and even larger. On one hand, an ordering of such a strength was never observed in AB-BLG. On the other hand, to fit this gap value into our framework, we need to assume large (~ 8.5 eV) pre-exponential factor in the expression for Δ_0 . This huge pre-exponential energy scale points toward certain weakness of a Hartree-Fock approach, partially explaining why the Hartree-Fock scheme produces unrealistically high order parameters values.

C. Fractional metallicity at weak doping

While a detailed study of doped AB-BLG is still in progress, several relevant observations about doping can already be made. For $0 < |V| < V_C$, the spectrum contains sectors with smaller and larger gaps (see Fig. 4). Upon doping, additional carriers enter the sector with the smallest gap first. This immediately implies that weak doping of the $n_+ = 3$, $n_- = 1$ phases stabilizes a quarter-metal state – that is, a metallic phase with complete polarization of the Fermi surface in both spin and valley quantum numbers^{30,38}.

At weak doping and finite V , the fate of the $n_{\pm} = 2$ state can follow either of two routes, depending on microscopic details. If the added electrons distribute evenly between the two (degenerate) low-gap sectors, a half-metal emerges²⁶. Alternatively, the doping itself may lift the sector degeneracy^{39–41}, resulting in a quarter-metal state.

This overall picture is partially consistent with the investigation of Ref. 26, whose the numerical mean-field framework was restricted to two independent order parameters, rather than four. As a result of this limitation, only the half-metallic phase was captured. Similar conclusions were drawn in Ref. 27 based on density-functional calculations.

VII. CONCLUSIONS

We formulated a simple mean field theory that describes electronic properties of undoped AB-BLG placed in transverse electric field. The model accounts not

only for short-range screened Coulomb interaction between electrons, but for the effects of the electrostatic energy associated with inter-layer polarization of the bilayer. We additionally introduce four independent order parameters, each order parameter is associated with a specific values of valley and spin quantum numbers. (Current-carrying order parameters are ignored from the start.) A set of four self-consistency equations is derived and solved. Despite physical dissimilarity, many ordered phases are found to be degenerate. We are able to classify these phases in accordance with their spin and valley projections. The external field induces transitions between various phases of the system. Single-electron gap is a non-monotonic function of the bias, and, for fixed bias, the gaps for different valleys and/or spin projections do not have to be the same. We map the phase diagram: at low bias, the ground state is likely to be layered antiferromagnet, at sufficiently large bias the bilayer is in the ferroelectric state. Comparison with experiment and other theoretical works is performed. The proposed framework may be relevant for study of doped AB-BLG.

Appendix A: Summation for MF energy

Let us evaluate the sum in Eq. (55)

$$E(D) = - \sum_{\mathbf{k}} \sqrt{\varepsilon_{\mathbf{k}}^2 + D^2}. \quad (\text{A1})$$

We use the following trick: we write $E(D) = E(0) + \int_0^D E'(\tilde{D})d\tilde{D}$, where $E(0)$ is a constant independent of D , while the derivative $E'(\tilde{D})$ is equal to

$$E'(\tilde{D}) = - \sum_{\mathbf{k}} \frac{\tilde{D}}{\sqrt{\varepsilon_{\mathbf{k}}^2 + \tilde{D}^2}} \approx -N_c \nu_0 \tilde{D} \ln \left(\frac{2t_0}{|\tilde{D}|} \right). \quad (\text{A2})$$

Indeed, if $D \ll t_0$, we obtain

$$\begin{aligned} \frac{1}{N_c} \sum_{\mathbf{k}} \frac{\tilde{D}}{\sqrt{\varepsilon_{\mathbf{k}}^2 + \tilde{D}^2}} &= \int \frac{S_0 d^2 \mathbf{k}}{(2\pi)^2} \frac{\tilde{D}}{\sqrt{\varepsilon_{\mathbf{k}}^2 + \tilde{D}^2}} = \\ \frac{t_0}{2\sqrt{3}\pi t^2} \int_0^{t_0} d\varepsilon \frac{\tilde{D}}{\sqrt{\varepsilon^2 + \tilde{D}^2}} &\approx \nu_0 \tilde{D} \ln \left(\frac{2t_0}{|\tilde{D}|} \right), \quad (\text{A3}) \\ \nu_0 &= \frac{t_0}{2\sqrt{3}\pi t^2}, \end{aligned}$$

and we derive Eq. (A2). If we then integrate over \tilde{D} , we get

$$\begin{aligned} E(D) &= E(0) - N_c \nu_0 \int_0^D \tilde{D} \ln \left(\frac{2t_0}{|\tilde{D}|} \right) d\tilde{D} \quad (\text{A4}) \\ &= E(0) - \frac{1}{2} N_c \nu_0 D^2 \left[\ln \left(\frac{2t_0}{|D|} \right) + \frac{1}{2} \right]. \end{aligned}$$

Appendix B: Variation energy minimization

and obtain

$$\begin{aligned} \frac{\partial \langle H_0 \rangle}{\partial [\hat{\Delta}_\xi]_{\sigma\sigma'}} &= \frac{\partial E_{\text{MF}}}{\partial [\hat{\Delta}_\xi]_{\sigma\sigma'}} + \sum_{\mathbf{k}} \langle [\hat{\Xi}_{\mathbf{k}\xi}^\dagger]_{\sigma'\sigma} \rangle + \quad (\text{B1}) \\ &\quad \sum_{\mathbf{k}} \text{Tr} \left(\frac{\partial \langle \hat{\Xi}_{\mathbf{k}\xi}^\dagger \rangle}{\partial [\hat{\Delta}_\xi]_{\sigma\sigma'}} \hat{\Delta}_\xi + \hat{\Delta}_\xi^\dagger \frac{\partial \langle \hat{\Xi}_{\mathbf{k}\xi}^\dagger \rangle}{\partial [\hat{\Delta}_\xi]_{\sigma\sigma'}} \right). \end{aligned}$$

The first two terms in the right-hand side of Eq. (B1) cancel each other, as Eq. (45) indicates. Therefore, the following is true

$$\langle H_0 \rangle = \sum_{\mathbf{k}} \text{Tr} \left(\hat{\Delta}_\xi \partial \langle \hat{\Xi}_{\mathbf{k}\xi}^\dagger \rangle + \hat{\Delta}_\xi^\dagger \partial \langle \hat{\Xi}_{\mathbf{k}\xi} \rangle \right), \quad (\text{B2})$$

where ∂X means $\partial X / \partial [\hat{\Delta}_\xi]_{\sigma\sigma'}$.

Next we differentiate $\langle H_{\text{int}} \rangle$, Eq. (58), and get

$$\begin{aligned} \partial \langle H_{\text{int}} \rangle &= \frac{\mathcal{E}_0}{4N_c} \left(\sum_{\mathbf{k}'\xi'} \text{Tr} \langle \hat{\Xi}_{\mathbf{k}'\xi'} \rangle + \text{Tr} \langle \hat{\Xi}_{\mathbf{k}'\xi'}^\dagger \rangle \right) \left(\sum_{\mathbf{k}} \text{Tr} \partial \langle \hat{\Xi}_{\mathbf{k}\xi} \rangle + \text{Tr} \partial \langle \hat{\Xi}_{\mathbf{k}\xi}^\dagger \rangle \right) - \quad (\text{B3}) \\ &\quad \frac{1}{N_c} \sum_{\mathbf{k}\mathbf{k}'} \left[\bar{\Gamma}_1 \text{Tr} \left(\langle \hat{\Xi}_{\mathbf{k}\xi}^\dagger \rangle \partial \langle \hat{\Xi}_{\mathbf{k}'\xi} \rangle + \langle \hat{\Xi}_{\mathbf{k}'\xi} \rangle \partial \langle \hat{\Xi}_{\mathbf{k}\xi}^\dagger \rangle \right) + \bar{\Gamma}_2 \text{Tr} \left(\langle \hat{\Xi}_{\mathbf{k}\xi}^\dagger \rangle \partial \langle \hat{\Xi}_{\mathbf{k}'\xi}^\dagger \rangle + \langle \hat{\Xi}_{\mathbf{k}\xi} \rangle \partial \langle \hat{\Xi}_{\mathbf{k}'\xi} \rangle \right) \right]. \end{aligned}$$

Combining the expressions for $\partial \langle H_0 \rangle$ and $\partial \langle H_{\text{int}} \rangle$, we derive

$$\partial E_{\text{var}} = \sum_{\mathbf{k}} \text{Tr} \left\{ \partial \langle \hat{\Xi}_{\mathbf{k}\xi}^\dagger \rangle \left[\hat{\Delta}_\xi - \frac{1}{N_c} \sum_{\mathbf{k}'} \bar{\Gamma}_1 \langle \hat{\Xi}_{\mathbf{k}'\xi} \rangle + \bar{\Gamma}_2 \langle \hat{\Xi}_{\mathbf{k}'\xi}^\dagger \rangle + \frac{\mathcal{E}_0}{4} \left(\text{Tr} \langle \hat{\Xi}_{\mathbf{k}'\xi} \rangle + \text{Tr} \langle \hat{\Xi}_{\mathbf{k}'\xi}^\dagger \rangle \right) \mathbb{I}_2 \right] \right\} + \text{c.c.} \quad (\text{B4})$$

If the expression in the square brackets vanishes, so does ∂E_{var} . Thus, the extrema of the variation energy corresponds to

$$\hat{\Delta}_\xi = \frac{1}{N_c} \sum_{\mathbf{k}'} \left(\bar{\Gamma}_1 \langle \hat{\Xi}_{\mathbf{k}'\xi} \rangle + \bar{\Gamma}_2 \langle \hat{\Xi}_{\mathbf{k}'\xi}^\dagger \rangle \right) - \frac{\mathcal{E}_0}{4} \mathbb{I}_2 \sum_{\xi'} \text{Tr} \langle \hat{\Xi}_{\mathbf{k}'\xi'} + \hat{\Xi}_{\mathbf{k}'\xi'}^\dagger \rangle. \quad (\text{B5})$$

To account for a finite $e\Phi$, we can shift $\hat{\Delta}_\xi$ by $(e\Phi/2)\mathbb{I}_2$

$$\hat{\Delta}_\xi(\Phi) = \hat{\Delta}_\xi + \frac{e\Phi}{2} \mathbb{I}_2. \quad (\text{B6})$$

Eqs. (B5) and (B6) can be considered as a self-consistency equations in our mean field approximation. Yet it is more convenient to invert them, expressing $\sum_{\mathbf{k}} \langle \hat{\Xi}_{\mathbf{k}\xi} \rangle$ and $\sum_{\mathbf{k}} \langle \hat{\Xi}_{\mathbf{k}\xi}^\dagger \rangle$ as functions of $\hat{\Delta}_\xi$ and $\hat{\Delta}_\xi^\dagger$. In this case only one non-linear term emerges in the self-consistency equation.

As a first step, we define

$$\hat{\mathcal{D}}_\xi = \hat{\Delta}_\xi + \frac{\mathcal{E}_0}{4} \frac{1}{N_c} \sum_{\mathbf{k}'\xi} \text{Tr} \langle \hat{\Xi}_{\mathbf{k}'\xi} + \hat{\Xi}_{\mathbf{k}'\xi}^\dagger \rangle \hat{\mathbb{I}}_2 - \frac{e\Phi}{2} \hat{\mathbb{I}}_2. \quad (\text{B7})$$

According to Eq. (B6), matrices $\hat{\mathcal{D}}_\xi$, $\hat{\mathcal{D}}_\xi^\dagger$ satisfy the following relations

$$\hat{\mathcal{D}}_\xi = \frac{1}{N_c} \sum_{\mathbf{k}'} \left(\bar{\Gamma}_1 \langle \hat{\Xi}_{\mathbf{k}'\xi} \rangle + \bar{\Gamma}_2 \langle \hat{\Xi}_{\mathbf{k}'\xi}^\dagger \rangle \right), \quad \hat{\mathcal{D}}_\xi^\dagger = \frac{1}{N_c} \sum_{\mathbf{k}'} \left(\bar{\Gamma}_1 \langle \hat{\Xi}_{\mathbf{k}'\xi}^\dagger \rangle + \bar{\Gamma}_2 \langle \hat{\Xi}_{\mathbf{k}'\xi} \rangle \right). \quad (\text{B8})$$

Solving these equations, we obtain

$$\frac{1}{N_c} \sum_{\mathbf{k}'} \langle \hat{\Xi}_{\mathbf{k}'\xi} \rangle = \frac{1}{\bar{\Gamma}_1^2 - \bar{\Gamma}_2^2} \left(\bar{\Gamma}_1 \hat{\mathcal{D}}_\xi - \bar{\Gamma}_2 \hat{\mathcal{D}}_\xi^\dagger \right), \quad \frac{1}{N_c} \sum_{\mathbf{k}'} \langle \hat{\Xi}_{\mathbf{k}'\xi}^\dagger \rangle = \frac{1}{\bar{\Gamma}_1^2 - \bar{\Gamma}_2^2} \left(\bar{\Gamma}_1 \hat{\mathcal{D}}_\xi^\dagger - \bar{\Gamma}_2 \hat{\mathcal{D}}_\xi \right). \quad (\text{B9})$$

Substituting definition (B7) in the latter equation, we derive after a straightforward algebra

$$\frac{(\bar{\Gamma}_1 + \bar{\Gamma}_2)}{N_c} \sum_{\mathbf{k}'} \langle \hat{\Xi}_{\mathbf{k}'\xi} \rangle = \frac{1}{\bar{\Gamma}_1 - \bar{\Gamma}_2} (\bar{\Gamma}_1 \hat{\Delta}_\xi - \bar{\Gamma}_2 \hat{\Delta}_\xi^\dagger) + \frac{\mathcal{E}_0}{4} \frac{1}{N_c} \sum_{\mathbf{k}'\xi} \text{Tr} \langle \hat{\Xi}_{\mathbf{k}'\xi'} + \hat{\Xi}_{\mathbf{k}'\xi'}^\dagger \rangle \hat{\mathbb{I}}_2 - \frac{e\Phi}{2} \hat{\mathbb{I}}_2, \quad (\text{B10})$$

Our task is not complete yet: the trace of $\langle \hat{\Xi} \rangle$ must be eliminated in the right-hand side of the latter formula. To express this trace in terms of the order parameter matrix, we take trace of both sides of Eq. (B10)

$$\frac{(\bar{\Gamma}_1 + \bar{\Gamma}_2)}{N_c} \sum_{\mathbf{k}'} \text{Tr} \langle \hat{\Xi}_{\mathbf{k}'\xi} \rangle = \frac{1}{\bar{\Gamma}_1 - \bar{\Gamma}_2} (\bar{\Gamma}_1 \text{Tr} \hat{\Delta}_\xi - \bar{\Gamma}_2 \text{Tr} \hat{\Delta}_\xi^\dagger) + \frac{\mathcal{E}_0}{2} \frac{1}{N_c} \sum_{\mathbf{k}'\xi'} \text{Tr} \langle \hat{\Xi}_{\mathbf{k}'\xi'} + \hat{\Xi}_{\mathbf{k}'\xi'}^\dagger \rangle - e\Phi. \quad (\text{B11})$$

Performing summation over ξ , we derive

$$\frac{(\bar{\Gamma}_1 + \bar{\Gamma}_2)}{N_c} \sum_{\mathbf{k}'\xi'} \text{Tr} \langle \hat{\Xi}_{\mathbf{k}'\xi'} + \hat{\Xi}_{\mathbf{k}'\xi'}^\dagger \rangle = \sum_{\xi'} \text{Tr} (\hat{\Delta}_{\xi'} + \hat{\Delta}_{\xi'}^\dagger) + 2\mathcal{E}_0 \frac{1}{N_c} \sum_{\mathbf{k}'\xi'} \text{Tr} \langle \hat{\Xi}_{\mathbf{k}'\xi'} + \hat{\Xi}_{\mathbf{k}'\xi'}^\dagger \rangle - 4e\Phi. \quad (\text{B12})$$

Therefore

$$\frac{1}{N_c} \sum_{\mathbf{k}'\xi'} \text{Tr} \langle \hat{\Xi}_{\mathbf{k}'\xi'} + \hat{\Xi}_{\mathbf{k}'\xi'}^\dagger \rangle = \frac{4e\Phi}{2\mathcal{E}_0 - \bar{\Gamma}_1 - \bar{\Gamma}_2} - \frac{1}{2\mathcal{E}_0 - \bar{\Gamma}_1 - \bar{\Gamma}_2} \sum_{\xi'} \text{Tr} (\hat{\Delta}_{\xi'} + \hat{\Delta}_{\xi'}^\dagger). \quad (\text{B13})$$

We can use Eq. (39) to express $\rho_{10} - \rho_{20}$ in terms of the order parameter as follows

$$\frac{\rho_{10} - \rho_{20}}{N_c} = -\frac{1}{N_c} \sum_{\mathbf{k}'\xi'} \text{Tr} \langle \hat{\Xi}_{\mathbf{k}'\xi'} + \hat{\Xi}_{\mathbf{k}'\xi'}^\dagger \rangle = -\frac{4e\Phi}{2\mathcal{E}_0 - \bar{\Gamma}_1 - \bar{\Gamma}_2} + \frac{1}{2\mathcal{E}_0 - \bar{\Gamma}_1 - \bar{\Gamma}_2} \sum_{\xi'} \text{Tr} (\hat{\Delta}_{\xi'} + \hat{\Delta}_{\xi'}^\dagger). \quad (\text{B14})$$

Substituting expression (B13) for the trace into the right-hand side of Eq. (B10), we establish

$$\frac{1}{N_c} \sum_{\mathbf{k}'} \langle \hat{\Xi}_{\mathbf{k}'\xi} \rangle = \frac{1}{\bar{\Gamma}_1^2 - \bar{\Gamma}_2^2} (\bar{\Gamma}_1 \hat{\Delta}_\xi - \bar{\Gamma}_2 \hat{\Delta}_\xi^\dagger) - \left\{ \frac{\mathcal{E}_0/4}{(\bar{\Gamma}_1 + \bar{\Gamma}_2)(2\mathcal{E}_0 - \bar{\Gamma}_1 - \bar{\Gamma}_2)} \sum_{\xi'} \text{Tr} (\hat{\Delta}_{\xi'} + \hat{\Delta}_{\xi'}^\dagger) - \frac{2\mathcal{E}_0 e\Phi}{(\bar{\Gamma}_1 + \bar{\Gamma}_2)(2\mathcal{E}_0 - \bar{\Gamma}_1 - \bar{\Gamma}_2)} \right\} \hat{\mathbb{I}}_2 - \frac{e\Phi}{2(\bar{\Gamma}_1 + \bar{\Gamma}_2)} \hat{\mathbb{I}}_2, \quad (\text{B15})$$

Thus

$$\begin{aligned} \frac{1}{N_c} \sum_{\mathbf{k}'} \langle \hat{\Xi}_{\mathbf{k}'\xi} \rangle &= \frac{1}{\bar{\Gamma}_1^2 - \bar{\Gamma}_2^2} (\bar{\Gamma}_1 \hat{\Delta}_\xi - \bar{\Gamma}_2 \hat{\Delta}_\xi^\dagger) - \frac{\mathcal{E}_0}{4(\bar{\Gamma}_1 + \bar{\Gamma}_2)(2\mathcal{E}_0 - \bar{\Gamma}_1 - \bar{\Gamma}_2)} \sum_{\xi'} \text{Tr} (\hat{\Delta}_{\xi'} + \hat{\Delta}_{\xi'}^\dagger) \hat{\mathbb{I}}_2 \\ &+ \frac{e\Phi}{2(2\mathcal{E}_0 - \bar{\Gamma}_1 - \bar{\Gamma}_2)} \hat{\mathbb{I}}_2. \end{aligned} \quad (\text{B16})$$

This is the desired relation between the anomalous averages and the order parameter.

We can use Eq. (52) and replace $\frac{1}{N_c} \sum_{\mathbf{k}'} \langle \hat{\Xi}_{\mathbf{k}'\xi} \rangle$ by the function of $\hat{\Delta}_\xi$ and $\hat{\Delta}_\xi^\dagger$. As a result we obtain non-linear equations, which can be solved to calculate the order parameter matrices $\hat{\Delta}_\xi$ and $\hat{\Delta}_\xi^\dagger$. If we assume that the order parameter is Hermitian, $\hat{\Delta}_\xi = \hat{\Delta}_\xi^\dagger$, then, such equations read as

$$\frac{1}{2N_c} \sum_{\mathbf{k}} \frac{\hat{\Delta}_\xi}{\sqrt{\varepsilon_{\mathbf{k}}^2 + \hat{\Delta}_\xi^2}} = \frac{\hat{\Delta}_\xi}{\bar{\Gamma}_1 + \bar{\Gamma}_2} - \frac{\mathcal{E}_0}{2(\bar{\Gamma}_1 + \bar{\Gamma}_2)(2\mathcal{E}_0 - \bar{\Gamma}_1 - \bar{\Gamma}_2)} \hat{\mathbb{I}}_2 \sum_{\xi'} \text{Tr} \hat{\Delta}_{\xi'} + \frac{e\Phi}{2(2\mathcal{E}_0 - \bar{\Gamma}_1 - \bar{\Gamma}_2)} \hat{\mathbb{I}}_2. \quad (\text{B17})$$

As the order parameter is Hermitian, we diagonalize it by a suitable unitary transformation. Thus, instead of two matrix equations (one per valley), four coupled scalar

equations emerge. Thus, after summation over \mathbf{k} and evident transformations we obtain from Eq. (B17) the self-consistency equation (64).

Appendix C: Effective constants for the Hartree-Fock calculations of Jung et al.

In this Appendix we provide a detailed explanation of how model parameters discussed in Sec. VI were extracted from the Hartree-Fock numerical data of Ref. 22, cited below as I.

Scrutinizing Figs. 5 and 6 of I, we establish that two transitions occur at external field of ~ 2.5 mV/nm and ~ 7.5 mV/nm. Multiplying these values by the inter-layer distance d , we find $e\Phi^* = 0.84$ meV, $e\Phi_C = 2.5$ meV. Similarly, one can establish that, between these transitions, the gap reaches its maximum value when the field is ~ 5 mV/nm. Thus, $e\Phi_{\max} = 1.7$ meV.

Using Eq. (93), we obtain

$$\frac{\mathcal{E}_0}{\bar{\Gamma}_1 + \bar{\Gamma}_2} = \frac{e\Phi^*}{\Delta_0} = 2.5 \times 10^{-2}, \quad (\text{C1})$$

where $\Delta_0 = 33$ meV was used, see Fig. 6 of I. That is, inequality (65) is drastically violated, making Λ and λ_{FE} negative. As we explained in Sec. IV A, negative λ_{FE} implies that the FE phase is metastable at vanishing bias. This conclusion is in agreement with data in Figs. 5 and 6 of I, which both show the FE branch extended to zero external field.

In the zero bias limit, the FE phase is characterized by $\Delta_{\text{FE}} = 25$ meV, visible in Fig. 6 of I. This, in conjunction with our Eq. (75), allows us to extract Λ :

$$\Lambda = \frac{1}{4} \ln \left(\frac{\Delta_{\text{FE}}}{\Delta_0} \right) = -6.9 \times 10^{-2}. \quad (\text{C2})$$

Note that, unlike inequality (78), restricting possible values of positive Λ , negative Λ range stretches from $-\infty$ to zero.

With Eq. (C1) in mind, one can approximate

$$|\Lambda| \approx \frac{\mathcal{E}_0}{\nu_0(\bar{\Gamma}_1 + \bar{\Gamma}_2)^2}, \quad (\text{C3})$$

and further derive

$$\gamma = (\bar{\Gamma}_1 + \bar{\Gamma}_2)\nu_0 \approx 0.36, \quad (\text{C4})$$

$$\bar{\varepsilon} = \nu_0 \mathcal{E}_0 \approx \Lambda \gamma^2 \approx 8.9 \times 10^{-3}. \quad (\text{C5})$$

This value of γ indicates that the Hartree-Fock model of I is in the weak-coupling limit. Estimate (C4) is of the same order as the value in our Eq. (78), but both values are not identical. Given quite dissimilar Coulomb interaction models employed in I and in the present paper, certain disparity between the two is very much expected.

Comparing (C5) with Eq. (88), one cannot help but notice that the values for $\bar{\varepsilon}$ are very much apart: our model's estimate for $\bar{\varepsilon}$ is almost two orders of magnitude larger than the value that follows from the data in I. The reason for such a discrepancy is unclear.

If we use the familiar mean field expression for the order parameter $\Delta_0 = We^{-2/\gamma}$, where W is a kind of ultraviolet cutoff, we find $W = 8.5$ eV. This pre-exponential factor is very large, much larger than the two-band theory cutoff of $2t_0$. Thus, within the two-band model, such a value of W cannot be justified.

Our Eq. (92) predicts that, when the zero-bias FE state is metastable and $|\Lambda|$ is small, the energy difference $\Delta E_{\text{FE}} > 0$, separating the FE state and the ground state, is $\Delta E_{\text{FE}} \approx 8|\Lambda|E_{\text{cond}}$, where $E_{\text{cond}} = N_c \nu_0 \Delta_0^2$ is the condensation energy. Thus, one can write $\Delta E_{\text{FE}}/E_{\text{cond}} \approx 8|\Lambda| \approx 0.56$. We can separately extract $E_{\text{cond}} \approx 5.17 \times 10^{-8}$ eV from table II of paper I, and $\Delta E_{\text{FE}} \approx 3 \times 10^{-8}$ eV from Fig. 5 of the same paper. Thus, numerical data allows us to calculate $\Delta E_{\text{FE}}/E_{\text{cond}} \approx 0.58$, in good agreement with the result derived from Eq. (92).

¹ A. Rozhkov, A. Sboychakov, A. Rakhmanov, and F. Nori, “Electronic properties of graphene-based bilayer systems,” *Phys. Rep.* **648**, 1 (2016).

² V. N. Kotov, B. Uchoa, V. M. Pereira, F. Guinea, and A. H. Castro Neto, “Electron-Electron Interactions in Graphene: Current Status and Perspectives,” *Rev. Mod. Phys.* **84**, 1067 (2012).

³ W. Bao, J. Velasco, F. Zhang, L. Jing, B. Standley, D. Smirnov, M. Bockrath, A. H. MacDonald, and C. N. Lau, “Evidence for a spontaneous gapped state in ultraclean bilayer graphene,” *PNAS* **109**, 10802 (2012).

⁴ J. Martin, B. E. Feldman, R. T. Weitz, M. T. Allen, and A. Yacoby, “Local Compressibility Measurements of Correlated States in Suspended Bilayer Graphene,” *Phys. Rev. Lett.* **105**, 256806 (2010).

⁵ R. T. Weitz, M. T. Allen, B. E. Feldman, J. Martin, and A. Yacoby, “Broken-Symmetry States in Doubly Gated Suspended Bilayer Graphene,” *Science* **330**, 812 (2010).

⁶ A. S. Mayorov, D. C. Elias, M. Mucha-Kruczynski, R. V. Gorbachev, T. Tudorovskiy, A. Zhukov, S. V. Morozov, M. I. Katsnelson, V. I. Fal'ko, A. K. Geim, et al., “Interaction-Driven Spectrum Reconstruction in Bilayer Graphene,” *Science* **333**, 860 (2011).

⁷ F. Freitag, J. Trbovic, M. Weiss, and C. Schönenberger, “Spontaneously Gapped Ground State in Suspended Bilayer Graphene,” *Phys. Rev. Lett.* **108**, 076602 (2012).

⁸ F. Freitag, M. Weiss, R. Maurand, J. Trbovic, and C. Schönenberger, “Homogeneity of bilayer graphene,” *Solid State Communications* **152**, 2053 (2012).

⁹ A. Veligura, H. J. van Elferen, N. Tombros, J. C. Maan, U. Zeitler, and B. J. van Wees, “Transport gap in suspended bilayer graphene at zero magnetic field,” *Phys. Rev. B* **85**, 155412 (2012).

¹⁰ J. Velasco Jr., L. Jing, W. Bao, Y. Lee, P. Kratz, V. Aji, M. Bockrath, C. Lau, C. Varma, R. Stillwell, et al., “Transport spectroscopy of symmetry-broken insulating states in

bilayer graphene,” *Nat. Nanotechnol.* **7**, 156 (2012).

¹¹ F. Freitag, M. Weiss, R. Maurand, J. Trbovic, and C. Schönenberger, “Spin symmetry of the bilayer graphene ground state,” *Phys. Rev. B* **87**, 161402 (2013).

¹² H. Zhou, T. Xie, A. Ghazaryan, T. Holder, J. R. Ehrets, E. M. Spanton, T. Taniguchi, K. Watanabe, E. Berg, M. Serbyn, et al., “Half- and quarter-metals in rhombohedral trilayer graphene,” *Nature* **598**, 429 (2021).

¹³ de la Barrera, C. Sergio, S. Aronson, Z. Zheng, K. Watanabe, T. Taniguchi, Q. Ma, P. Jarillo-Herrero, and R. Ashoori, “Cascade of isospin phase transitions in Bernal-stacked bilayer graphene at zero magnetic field,” *Nat. Phys.* **18**, 771 (2022).

¹⁴ A. M. Seiler, F. R. Geisenhof, F. Winterer, K. Watanabe, T. Taniguchi, T. Xu, F. Zhang, and R. T. Weitz, “Quantum cascade of correlated phases in trigonally warped bilayer graphene,” *Nature* **608**, 298 (2022).

¹⁵ H. Zhou, L. Holleis, Y. Saito, L. Cohen, W. Huynh, C. L. Patterson, F. Yang, T. Taniguchi, K. Watanabe, and A. F. Young, “Isospin magnetism and spin-polarized superconductivity in Bernal bilayer graphene,” *Science* **375**, 774 (2022).

¹⁶ E. McCann, D. S. Abergel, and V. I. Fal’ko, “Electrons in bilayer graphene,” *Solid State Commun.* **143**, 110 (2007), exploring graphene.

¹⁷ R. Nandkishore and L. Levitov, “Dynamical Screening and Excitonic Instability in Bilayer Graphene,” *Phys. Rev. Lett.* **104**, 156803 (2010).

¹⁸ R. Nandkishore and L. Levitov, “Quantum anomalous Hall state in bilayer graphene,” *Phys. Rev. B* **82**, 115124 (2010).

¹⁹ O. Vafek, “Interacting fermions on the honeycomb bilayer: From weak to strong coupling,” *Phys. Rev. B* **82**, 205106 (2010).

²⁰ O. Vafek and K. Yang, “Many-body instability of Coulomb interacting bilayer graphene: Renormalization group approach,” *Phys. Rev. B* **81**, 041401 (2010).

²¹ Y. Lemonik, I. L. Aleiner, C. Toke, and V. I. Fal’ko, “Spontaneous symmetry breaking and Lifshitz transition in bilayer graphene,” *Phys. Rev. B* **82**, 201408 (2010).

²² J. Jung, F. Zhang, and A. H. MacDonald, “Lattice theory of pseudospin ferromagnetism in bilayer graphene: Competing interaction-induced quantum Hall states,” *Phys. Rev. B* **83**, 115408 (2011).

²³ V. Cvetkovic, R. E. Throckmorton, and O. Vafek, “Electronic multicriticality in bilayer graphene,” *Phys. Rev. B* **86**, 075467 (2012).

²⁴ A. L. Rakhmanov, A. V. Rozhkov, A. O. Sboychakov, and F. Nori, “Instabilities of the AA-Stacked Graphene Bilayer,” *Phys. Rev. Lett.* **109**, 206801 (2012).

²⁵ M. Kharitonov, “Antiferromagnetic state in bilayer graphene,” *Phys. Rev. B* **86**, 195435 (2012).

²⁶ J. Yuan, D.-H. Xu, H. Wang, Y. Zhou, J.-H. Gao, and F.-C. Zhang, “Possible half-metallic phase in bilayer graphene: Calculations based on mean-field theory applied to a two-layer Hubbard model,” *Phys. Rev. B* **88**, 201109 (2013).

²⁷ J. Baima, F. Mauri, and M. Calandra, “Field-effect-driven half-metallic multilayer graphene,” *Phys. Rev. B* **98**, 075418 (2018).

²⁸ L. Brey and H. A. Fertig, “Gapped phase in AA-stacked bilayer graphene,” *Phys. Rev. B* **87**, 115411 (2013).

²⁹ A. O. Sboychakov, A. L. Rakhmanov, A. V. Rozhkov, and F. Nori, “Metal-insulator transition and phase separation in doped AA-stacked graphene bilayer,” *Phys. Rev. B* **87**, 121401 (2013).

³⁰ A. O. Sboychakov, A. L. Rakhmanov, A. V. Rozhkov, and F. Nori, “Bilayer graphene can become a fractional metal,” *Phys. Rev. B* **103**, L081106 (2021).

³¹ F. R. Geisenhof, F. Winterer, A. M. Seiler, J. Lenz, F. Zhang, and R. T. Weitz, “Impact of Electric Field Disorder on Broken-Symmetry States in Ultraclean Bilayer Graphene,” *Nano Lett.* **22**, 7378 (2022).

³² A. O. Sboychakov, A. V. Rozhkov, and A. L. Rakhmanov, “Triplet superconductivity and spin density wave in biased AB bilayer graphene,” *Phys. Rev. B* **108**, 184503 (2023).

³³ Y. Lemonik, I. Aleiner, and V. I. Fal’ko, “Competing nematic, antiferromagnetic, and spin-flux orders in the ground state of bilayer graphene,” *Phys. Rev. B* **85**, 245451 (2012).

³⁴ H. Min, G. Borghi, M. Polini, and A. H. MacDonald, “Pseudospin magnetism in graphene,” *Phys. Rev. B* **77**, 041407 (2008).

³⁵ A. V. Rozhkov, A. O. Sboychakov, and A. L. Rakhmanov, “Ordered states in AB bilayer graphene in a SU(4)-symmetric model,” *Phys. Rev. B* **111**, 205421 (2025).

³⁶ A. V. Rozhkov, A. O. Sboychakov, and A. L. Rakhmanov, “Ordering in the SU(4)-symmetric model of AA bilayer graphene,” *Phys. Rev. B* **108**, 205153 (2023).

³⁷ F. Zhang, J. Jung, G. A. Fiete, Q. Niu, and A. H. MacDonald, “Spontaneous Quantum Hall States in Chirally Stacked Few-Layer Graphene Systems,” *Phys. Rev. Lett.* **106**, 156801 (2011).

³⁸ A. L. Rakhmanov, A. V. Rozhkov, A. O. Sboychakov, and F. Nori, “Half-metal and other fractional metal phases in doped AB bilayer graphene,” *Phys. Rev. B* **107**, 155112 (2023).

³⁹ L. V. Keldysh and Y. V. Kopaev, “Possible instability of the semimetallic state toward Coulomb interaction,” *Sov. Phys. Solid State* **6**, 2219 (1965).

⁴⁰ L. V. Keldysh and Y. V. Kopaev, in *Selected Papers of Leonid V Keldysh* (World Scientific, 2024), pp. 41–46.

⁴¹ Y. I. Rodionov, A. V. Rozhkov, M. E. S. Beck, A. O. Sboychakov, K. I. Kugel, and A. L. Rakhmanov, “Nesting-driven ferromagnetism of itinerant electrons,” *Phys. Rev. B* **112**, 205129 (2025).